





## Article

# Experimental Validation of Electrothermal and Aging Parameter Identification for Lithium-Ion Batteries

Francesco Conte <sup>1,\*</sup> , Marco Giallongo <sup>2</sup> , Daniele Kaza <sup>3</sup>, Gianluca Natrella <sup>3</sup>, Ryohei Tachibana <sup>4</sup>, Shinji Tsuji <sup>4</sup>, Federico Silvestro <sup>3</sup>  and Giovanni Vichi <sup>2</sup> 

<sup>1</sup> Department of Engineering, Campus Bio-Medico University of Rome, Via Alvaro del Portillo 21, 00128 Roma, Italy

<sup>2</sup> Yanmar R&D Europe SRL, Viale Galileo 3/A, 50125 Firenze, Italy; marco\_giallongo@yanmar.com (M.G.); giovanni\_vichi@yanmar.com (G.V.)

<sup>3</sup> Dipartimento di Ingegneria Navale, Elettrica, Elettronica e delle Telecomunicazioni, Università degli Studi di Genova, Via all'Opera Pia 11a, 16145 Genova, Italy; daniele.kaza@edu.unige.it (D.K.); gianluca.natrella@edu.unige.it (G.N.); federico.silvestro@unige.it (F.S.)

<sup>4</sup> Yanmar Holdings Co., Ltd., 2481 Umegahara, Maibara 5218511, Shiga, Japan; ryohei\_tachibana@yanmar.com (R.T.); shinji\_tsuji@yanmar.com (S.T.)

\* Correspondence: f.conte@unicampus.it

**Abstract:** Modeling and predicting the long-term performance of Li-ion batteries is crucial for the effective design and efficient operation of integrated energy systems. In this paper, we introduce a comprehensive semi-empirical model for Li-ion cells, capturing electrothermal and aging features. This model replicates the evolution of cell voltage, capacity, and internal resistance, in relation to the cell actual operating conditions, and estimates the ongoing degradation in capacity and internal resistance due to the battery use. Thus, the model articulates into two sub-models, an electrothermal one, describing the battery voltage, and an aging one, computing the ongoing degradation. We first propose an approach to identify the parameters of both sub-models. Then, we validate the identification procedure and the accuracy of the electrothermal and aging models through an experimental campaign, also comprising two real cycle load tests at different temperatures, in which real measurements collected from real Li-ion cells are used. The overall model demonstrates good performances in simulating battery characteristics and forecasting degradation. The results show a Mean Absolute Percentage Error (MAPE) lower than 1% for battery voltage and capacity, and a maximum absolute error on internal resistance that is on par with the most up-to-date empirical models. The proposed approach is therefore well-suited for implementation in system modeling, and can be employed as an informative tool for enhancing battery design and operational strategies.

**Keywords:** Li-ion battery degradation; semi-empirical model; parameter identification; performance and lifetime prediction



**Citation:** Conte, F.; Giallongo, M.; Kaza, D.; Natrella, G.; Silvestro, F.; Tachibana, R.; Tsuji, S.; Vichi, G. Experimental Validation of Electrothermal and Aging Parameter Identification for Lithium-Ion Batteries. *Energies* **2024**, *17*, 2269. <https://doi.org/10.3390/en17102269>

Academic Editor: Aurelio Somà

Received: 21 March 2024

Revised: 30 April 2024

Accepted: 6 May 2024

Published: 8 May 2024



**Copyright:** © 2024 by the authors. Licensee MDPI, Basel, Switzerland. This article is an open access article distributed under the terms and conditions of the Creative Commons Attribution (CC BY) license (<https://creativecommons.org/licenses/by/4.0/>).

## 1. Introduction

The relentless pursuit of sustainable energy solutions has led to the widespread adoption of lithium-ion batteries (LiBs) as a primary energy storage technology in numerous applications, ranging from portable electronics to transportation and renewable energy systems [1–4]. The energy landscape is transitioning from traditional fossil fuel-based systems to distributed solutions powered by renewable sources, notably wind and photovoltaic energy [5]. Nevertheless, the intermittent nature of renewable sources presents challenges to the reliable and stable operation of energy grids.

The primary drivers behind the LiBs being widespread are their exceptional technical characteristics, which include high energy and power densities, impressive efficiency, and minimal self-discharge rates in comparison to their counterparts, such as NiCd, NiMH, and Lead Acid batteries [6–8]. To harness these advantages effectively, LiBs must operate

under the supervision of a battery management system (BMS). The BMS plays a crucial role in ensuring that the battery operates safely within its designated temperature and state of charge (SOC) parameters. For LiBs, the temperature of the cells is not only influential in affecting the open circuit voltage (OCV), internal resistance, and available capacity, but it can also cause rapid battery degradation and even thermal runaway if the battery is operated beyond a specified temperature threshold. To maintain the battery within its safe operational range under all conditions, an electrothermal battery model is crucial. Such a model must comprehensively represent both the electrical and thermal behaviors of Li-ion cells, guaranteeing that the battery temperature remains well within acceptable limits throughout its operation [9–11].

While LiBs have undoubtedly revolutionized the way we store and utilize energy, their long-term performance and reliability remain central challenges [5]. Over time, LiBs inevitably degrade due to a multitude of complex factors, collectively referred to as aging phenomena. Understanding and identifying the key mechanisms behind LiB aging is fundamental to extend their lifespan, enhance their safety, and optimize their performance. Battery aging models can be classified according to the methodology adopted into three groups hereby listed in descending order of physical–chemical knowledge and computational effort, and in ascending order of experimental test requirement and applicability: electrochemical models, semi-empirical models, and data-driven models.

Electrochemical aging models require the knowledge of several physical and chemical parameters of the cell, different for each type of LiBs and very difficult to measure. However, they need a few experimental tests as the model is very detailed. In [12], an aging formulation for NCA/graphite Li-ion cells that include heterogeneous dual-layer solid electrolyte interphase and lithium-plating aging mechanisms with porosity evaluation is proposed. The implemented model belongs to the category of electrochemical ones and requires an extensive knowledge of the chemical and physical aspects of the cell. More than 60 parameters are required to model the aging of the cell, of which 14 were not known and have been estimated bringing to End of Life (EoL) only one cell. The model captures the cell capacity fade with an accuracy of 98% goodness-of-fit error. Another example of an electrochemical aging model is [13] which develops a single particle-based degradation model [14] by including the physics of capacity and voltage degradation phenomena. The model has 35 parameters, and it captures the capacity fade and voltage profile as functions of cycle number with a Root Mean Square Error (RMSE) of 1.03%.

Data-driven aging models, on the contrary, do not require any physical and chemical knowledge of the battery, and can be extended to every type of LiB. Their major drawback is the extensive experimental campaign that has to be made in order to develop the model, which degrades several batteries, thus increasing the operational costs. In a set of two papers [15,16], a data-driven model to estimate the capacity degradation of lithium-ion cells is presented. The papers investigate calendar and cycling aging, and introduce a data-driven aging model for Li-ion batteries under the Gaussian process framework. To build the calendar aging model, 32 cells were tested, while the cycling aging model was built on the results of experiments on 124 cells. The calendar and cycling aging models returned a Mean Absolute Error (MAE) of 0.58% and 1.04%, respectively. In [17], a feed-forward migration neural network is proposed to predict LiBs' aging trajectories. First, a base model that describes the capacity decay over time is established from the existing battery aging data set. Then, the base model is transformed by an input–output slope and bias correction method structure to capture the degradation of the target cell. To enhance the model's nonlinear transfer capability, the model is further integrated into a four-layer neural network. A total of eight batteries were utilized and brought to their EoL, and the model always returned a RMSE lower than 2.5%. In [18], a multivariable fractional polynomial regression approach is proposed to model the degradation of LiBs. In [19], a data-driven approach is proposed to forecast LiBs' state of health (SOH) and SOC under constant current discharge conditions.

Semi-empirical aging models stand in the middle between electrochemical and data-driven models, balancing complexity, computational effort, applicability, and data requirements; furthermore, they can be applied to different types of LiBs [20]. In [21], a method to estimate the battery SOH and SOC with a semi-empirical approach is proposed. The developed model uses three parameters, two of which are time-variant. One battery is repeatedly charged and discharged till its EoL and three others undergo a dynamic stress test protocol, each one at a different temperature. The validation results show a correlation coefficient of 0.9. In [22], a semi-empirical LiB degradation model assessing the battery cell life loss from operating profiles is proposed. The model takes as input the battery Depth of Discharge (DoD), SOC, and temperature, and provides an offline estimation of the SOH. Experiments were run on a total of eight batteries and the results showed a SOH estimation error near 3%. In [20], a semi-empirical model for battery capacity and resistance degradations is proposed, based on physical equations from fatigue theory and equivalent cycle counting. The model takes as input the ambient temperature, the battery SOC, and current, and it is interfaced with an electrochemical model of a LiB that evaluates the battery temperature evolution from the working conditions and the ambient temperature [11]. The model is validated using two types of Li-ion cells (LFP and NMC) and simulation results show an error within  $\pm 1.5\%$  compared to experimental results.

Semi-empirical and data-driven aging models can be integrated to create hybrid models. An example of a semi-empirical/data-driven aging model is [23], where a robust SOH estimation method is proposed. The developed model presents four parameters, of which two are estimated through curve fitting, one is predicted by training a neural network, and one is obtained through Gaussian process regression. Tests are run on five batteries (three LFPs with 32 cells each and two NMCs with 40 cells each) cycled according to four different categories of tests, i.e., (1) standard cycling at different C-rates and temperatures, (2) standard calendar at different SOCs, (3) combination of cycling and calendar, and (4) combination of realistic working conditions. For standard cycling tests, the RMSE is below 4% for most of the groups of batteries; for the standard calendar, the RMSE is lower than 2%; for the combination of cycling and testing, the average RMSE is 1.21%; for the combination of realistic working conditions, the average RMSE is 1.53%.

In this paper, we present a LiB electrothermal model (EM) that returns the battery voltage and capacity as functions of the battery temperature, and interfaces with a LiB semi-empirical aging model (AM) that forecasts online the battery capacity and resistance evolution. Moreover, we propose a method to identify the parameters of the two models and validate the results on cross-validating tests. The main contributions of this work can be summarized as follows:

1. Development of a comprehensive LiB model able to represent the battery voltage, capacity, and resistance according to battery temperature and degradation, to forecast their evolution over time and/or to be easily integrated with a BMS.
2. A suitably developed method to identify the parameters of the electrothermal and aging parameters of the LiB model.
3. An extensive experimental validation realized by using measurements collected from real Li-ion cells and real battery-use profiles.

It is worth noticing that the proposed LiB model is an enhanced version of existing electrothermal and aging models. Specifically, the EM is formulated based on the models in [11,24,25], while the AM starts from the one presented in [20]. However, as we will specifically clarify in Sections 3.3 and 4.3, in this paper we introduce two main improvements: the formal inclusion of the relation between the maximum theoretical discharge capacity, used in the EM, and the battery nominal capacity, used in the AM; and the generalization of the aging parameter identification procedure to the case of multiple experimental measurements for each aging condition.

The remainder of this paper is organized as follows: Section 2 introduces the problem and the experimental dataset, Section 3 describes the LiBs models, Section 4 presents

the parameter identification methodology, Section 5 presents the results, and Section 6 summarizes the paper conclusions.

## 2. Problem Statement and Experimental Dataset

The principal objective of this paper is to experimentally validate a model able to reproduce the operation due to aging of LiBs. Among the observable aging-related phenomena, we focus on two aspects: capacity fade and internal resistance increase, two phenomena that lead to reduced availability of energy storage, power fade, and reduced round trip efficiency. To model these phenomena, we will introduce and validate a semi-empirical AM. In order to obtain a complete representation of the battery behavior, the AM has to face an EM that returns the battery voltage, capacity, and internal resistance in the function of the current and temperature. Therefore, we will also introduce and validate an EM. The final result will be the Whole Battery Model (WBM) obtained by coupling the EM and the AM.

The purpose of developing the WBM lies in several potential practical applications. Indeed, the WBM can be used in electric vehicles [26,27] or in stationary applications, such as microgrids [28,29] and grid-level storage systems [30], to allow the real-time monitoring of the battery SOH or to be integrated into optimal battery management algorithms. Moreover, the WBM can also be used to perform simulations in the design phase of new devices employing LiBs.

Regardless of the final use of the WBM, this paper focuses on the offline preliminary phase, where the WBM is identified and validated using a properly defined set of experimental measurements on the same battery type that will be used in the real application. Any stage after the WBM validation is beyond the scope of the paper.

The proposed procedure to identify and validate the WBM is shown in Figure 1. We design three sets of experimental tests: Experiment 1, to identify the parameters of the EM; Experiment 2, to identify the parameters of the AM; Experiment 3, to realize the validation. In Section 2.1 we detail the three experiments. The EM and AM parameter identification procedures are described in Section 4.1 and Section 4.2, respectively. Finally, validation results are reported in Section 5.

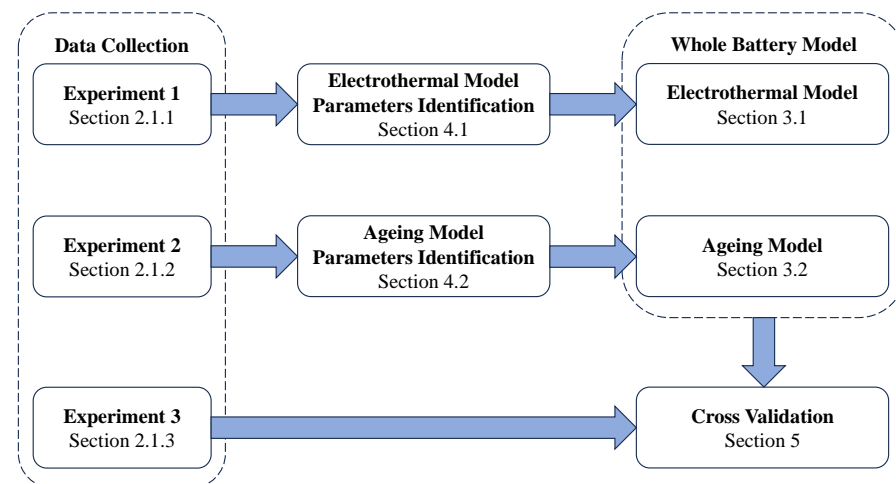


**Figure 1.** Flowchart of the adopted procedure to identify and validate the parameters of the WBM.

### 2.1. Experiment Description

To properly define the set of experimental tests, we considered that the following operating conditions have an impact on the LiBs' electrothermal behavior and on the capacity fade and internal resistance growth [31]:

- Charge rate;
- Discharge rate;
- Battery temperature;
- DoD.

The current rate affects the terminal voltage and internal potential, leading to side reactions that reduce battery life. Excessive current accelerates active material fatigue, damages the structure, and disrupts current distribution, potentially causing local lithium plating. Fast charging, in particular, can lead to lithium deposition, further affecting battery life. Temperature affects various reactions within the battery, with higher temperatures increasing side reactions and potentially causing thermal runaway (the optimal working range for most commercial LiBs is typically in the range of 15–35 °C). Finally, in LiBs, cycling within a certain DoD range is critical. Initially, increasing DoD improves battery life by lowering the average SOC and anode potential. However, high DoD leads to phase changes in cathode and anode materials, causing structural and volume changes and significantly reducing battery life.

Therefore, the three experimental tests detailed in the following have been designed and carried out taking into account the above-listed four operating conditions. During all tests, battery temperature, current, and voltage were constantly monitored and logged with a corresponding timestamp. Tests were carried out on Samsung INR21700-50E (Samsung SDI Co. Ltd., Yongin, Gyeonggi-do, Republic of Korea.) lithium-ion cells [32], assuming as given from the datasheet the cut-off voltage  $V_{cut-off}$  (V), the full capacity voltage  $V_{full}$  (V), and the nominal capacity  $Q$  (Ah) in fresh battery conditions. However, it should be pointed out that the experimental discharge curves performed on these cells showed a lower capacity than the one declared in [32].

It is finally worth remarking that all experimental data have been provided by Yanmar Holdings Co., Ltd. (Maibara, Japan) [33] based on their experience in using LiBs in off-road vehicles and industrial applications.

#### 2.1.1. Experiment 1

The purpose of Experiment 1 is to characterize the battery EM. To this end, a fresh battery was discharged three times from full capacity at constant current (CC) to reach the cut-off voltage ( $V_{cut-off}$ ) with the same C-rate. Each discharge was carried out at a different temperature, i.e., 0 °C, 25 °C, 50 °C, and at the 0.5C rate. Before discharging at CC, the battery was brought to 100% SOC (which the full capacity voltage  $V_{full}$  is related to) and the test temperature was set. Then, the battery was discharged at the 0.5C rate, meaning that in two hours the whole battery nominal capacity  $Q$  was transferred and the output voltage was registered with a sampling time of 1 s. Once the cut-off voltage  $V_{cut-off}$  was reached, the battery was rested for 10 min before being charged at 0.5C to 100% SOC. Then, the temperature was updated for the following discharge (the second and the third ones).

#### 2.1.2. Experiment 2

Experiment 2 is a set of cycle tests, detailed in Table 1, suitably designed to investigate the effects of the four stress factors (charge rate, discharge rate, battery temperature, and DoD) on capacity fade and internal resistance increase. A cycle test consisted of repeating charge/discharge cycles at specific battery temperature conditions, with established charge and discharge rates, and within a specific SOC range. Every time the top and bottom ends of the SOC range were reached, the battery was rested for 10 min. To define the tests listed in Table 1, a test matrix was organized with two charge rates (0.5C and 1C), two discharge rates (1C and 2C), two battery temperatures (25 °C and 40 °C), and two DoDs (100% and 80%). Considering one of the two test values for each of the four stress factors as reference, five cycle tests were carried out: one setting all stress factors at the reference values (cycle test #1) and four by setting one stress factor at a non-reference value (cycle tests #2–#5). Then, to further investigate the effect of the DoD at different starting SOC, a sixth cycle test was realized (cycle test #6).



**Table 1.** Cycle aging tests composing the Experiment 2 set. For the stress conditions, bold values are the non-reference values.

Test #	Battery Cells	Temp.	Charge Rate	Discharge Rate	SOC Range
1	3	25 °C	0.5C	1C	0–100%
2	3	<b>40 °C</b>	0.5C	1C	0–100%
3	1	25 °C	<b>1C</b>	1C	0–100%
4	1	25 °C	0.5C	<b>2C</b>	0–100%
5	1	25 °C	0.5C	1C	<b>10–90%</b>
6	1	25 °C	0.5C	1C	<b>20–100%</b>

To monitor the battery degradation, at the beginning and every 50 cycles a capacity measurement and a resistance measurement were conducted during each cycle test. Furthermore, cycle tests #1 and #2 were conducted on three different battery cells each, while all the other cycle tests were conducted on just one battery cell. The data of one each of the three cells subject to cycle tests #1 and #2 were used for the validation, namely cycle test #1-3 and cycle test #2-3, whereas the data of the other two cells were used for the identification of the parameters. Each test was suspended after the battery hit the EoL, which in this work is defined as the condition at which the battery capacity reaches 80% of the battery capacity at the Beginning of Life (BoL). The capacity measurement consists of repeating the same discharge procedure of Experiment 1 with a discharge current of 0.98 A (approximately 0.2C rate) and monitoring the amount of extracted capacity to reach a voltage of  $V_{cut-off}$  from a voltage of  $V_{full}$ .

Figure 2 illustrates how the internal resistance was computed. Two discharge current steps were applied to the cell, i.e.,  $I_1$  at 1C for 1 s and  $I_2$  at 0.2C for 5 s, such that the extracted capacity was the same. The steady-state values of the terminal voltage were measured after the two current steps, i.e.,  $V_1$  after  $I_1$  and  $V_2$  after  $I_2$ . Then, the resistance was estimated as the ratio between the differences between voltage values and the difference between current values in the two testing conditions as follows:

$$R = \frac{V_1 - V_2}{I_2 - I_1} \quad (1)$$

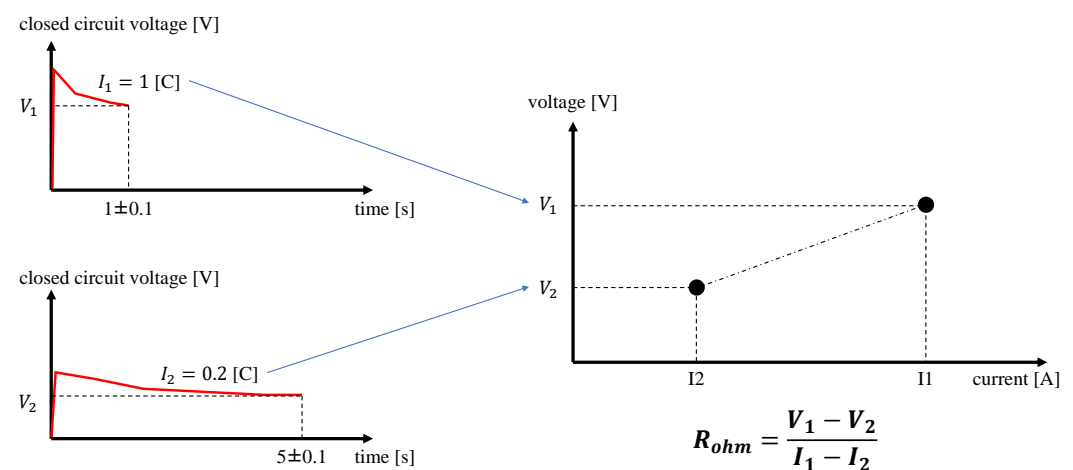


**Figure 2.** Description of tests for ohmic resistance measurement. **Left:** steady-state voltage measurements:  $V_1$  after a current discharge step  $I_1$  at 1C for 1 s (**top**),  $V_2$  after a current step at 0.2C for 5 s (**bottom**). **Right:** the ohmic resistance is computed as the ratio between the differences of the voltage measurements and the difference of the current step magnitudes.

### 2.1.3. Experiment 3

Experiment 3 is a set of tests used to validate the WBM. To this end, two real load cycles were designed, namely Pattern A, at 0 and 25 °C, and Pattern B, at 25 °C, to validate the AM model. Moreover, as anticipated in Section 2.1.2, one each of the three cycle tests #1 and #2, i.e., #1-3 and #2-3, were also used to validate the battery AM parameters, together with a test that we referred to as Append 5, which consists of the same operations of cycle test #5 run at 40 °C. The validation of the EM was carried out using discharge tests identical to those in Experiment 1 and on discharge tests for battery capacity measurements performed during the Pattern A test, Pattern B test, cycle test #1-3, cycle test #2-3, and Append 5 test. In particular, the discharge tests identical to those of Experiment 1 were conducted at 0, 10, 25, 40, and 50 °C on fresh batteries at the 0.5C rate, while the other tests were also used to validate the battery EM parameters at different levels of battery age and to cross-validate the WBM. As previously mentioned in Section 2.1.2, the capacity measurements consist of full discharge test at 0.98 A.

Regarding the validation of the AM, the details of Pattern A and Pattern B are given in the following. Figure 3 shows the diagram of Pattern A: the top graph is the profile current applied to the battery, with positive values meaning charging; on the bottom the estimated evolution of the battery SOC is shown. Each timestamp lasts 1 h, except for the 12th that lasts the time needed to reach the voltage  $V_{full}$ , and for the 24th timestamp that lasts the necessary time to discharge 840 mAh along the 22nd, 23rd, and 24th timestamps. Pattern B is shown in Figure 4. Figure 4a describes the general cycle that lasts around 19 h: on top we have the current applied to the battery cell, with positive values referring to charge operations; on the bottom the estimated SOC evolution is given. The discharges highlighted in Figure 4a are not operated under CC conditions and consist of the repetition of the pattern detailed in Figure 4b; in particular, the same pattern, lasting 20 min, is repeated along test Pattern B once for 2.5 h and, later, once for the necessary time to reach  $V_{cut-off}$ . The cycle composing Pattern B ends with a full CC-CV charge to be repeated.

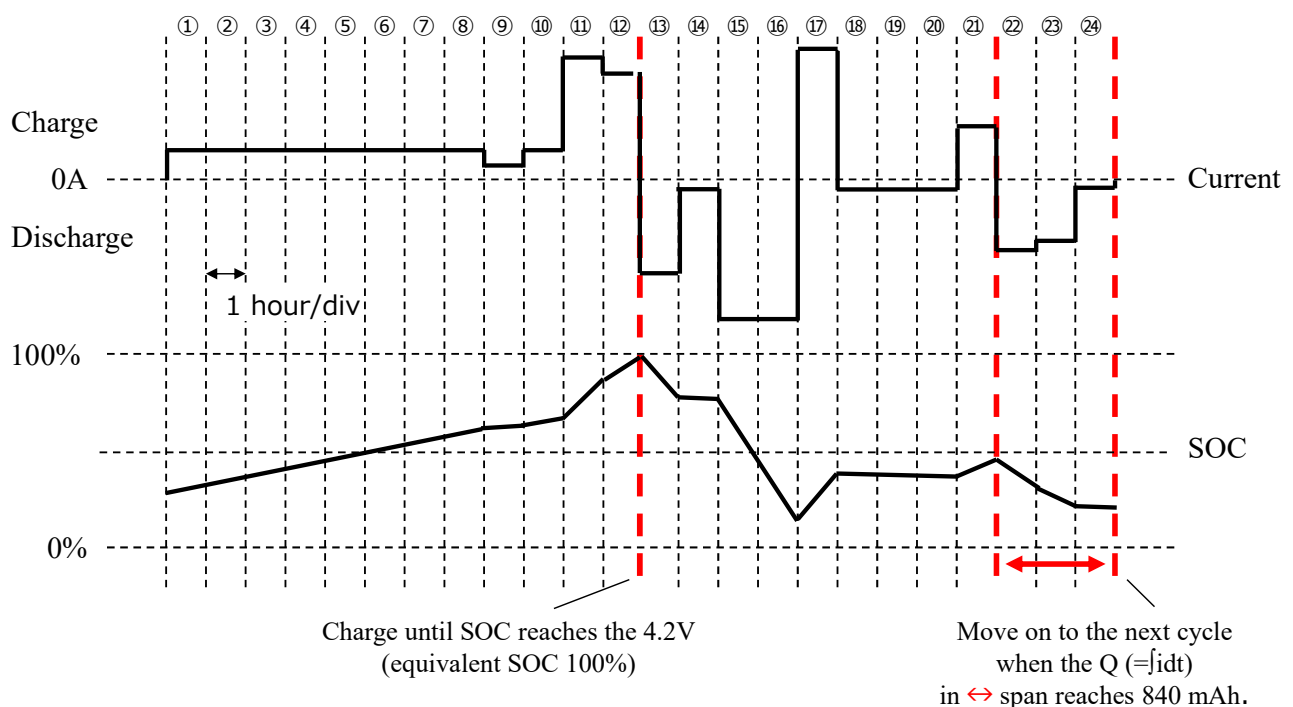


**Figure 3.** Pattern A validation test; on the top there is the current profile (positive value corresponds to charging, negative value to discharging) and on the bottom the estimated SOC profile. The test lasts around 24 h.

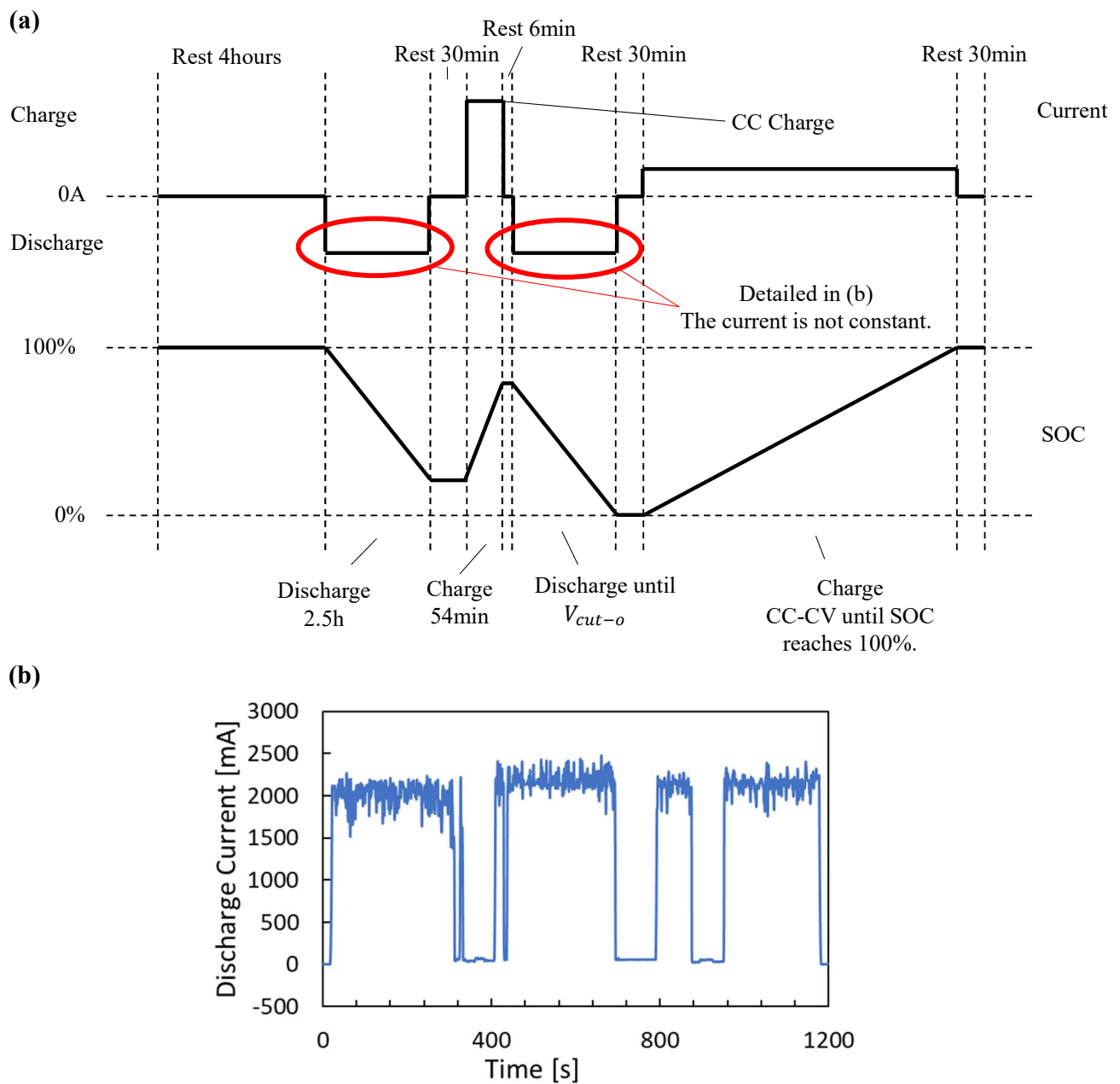


**Figure 4.** Pattern B validation test. (a) shows the general profile; on the top there is the current profile (positive value refers to charge) and on the bottom the estimated SOC profile; (b) details the discharge profile that lasts 20 min and is repeated to cover 2.5 h (first discharge in (a)) and to reach  $V_{cut-off}$  (second discharge in (a)). The test lasts around 19 h.

### 3. Battery Model

This section presents the WBM, whose basic diagram is shown in Figure 5. It consists of two sub-models, the EM and the AM. The EM in turn consists of two main blocks: Block E1 and Block E2.

Block E2 is the electrothermal sub-model, which computes the battery voltage  $V_b$  (V), given the battery current  $i$  (A), positive if charging, and the actual values of: battery maximum capacity  $Q_b$  (Ah); battery resistance  $R$  ( $\Omega$ ); and three other model parameters,  $E_0$ ,  $K$ , and  $A_b$ , introduced in the following.

Block E1 is the thermal sub-model, which computes the battery maximum capacity and resistance at BoL,  $Q_b^{BoL}$ , and  $R^{BoL}$ , and the values of  $E_0$ ,  $K$ , and  $A_b$ , in the function of the battery temperature  $T$ .



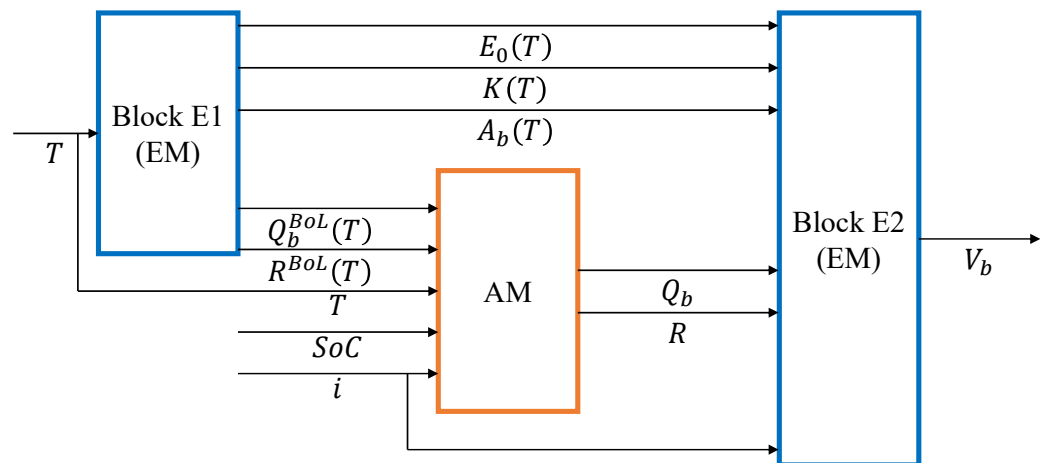


**Figure 5.** Basic block scheme of the WBM.

The AM quantifies the ongoing battery degradation and returns  $Q_b$  and  $R$  from their corresponding values at BoL, as functions of the four stress variables: charge rate, discharge rate, battery temperature, and DoD.

### 3.1. Battery Electrothermal Model

The proposed EM model is based on the modified Shepherd curve fitting mode [34,35], where an additional term (voltage polarization) is added to the battery voltage formulation to better represent the effect of SOC on the battery open circuit voltage. Also, to represent the battery dynamics, the battery current is delayed through a low-pass filter accounting for the polarization resistance. As mentioned before and shown in Figure 5, the EM is composed of Block E1 and Block E2. In the following, we detail these two blocks, starting with Block E2.

#### 3.1.1. Block E2

For a LiB type, the battery voltage  $V_b$  is expressed as follows:

$$V_b = E_0 - K \frac{Q_b}{Q_b - q(t)} q(t) + Ri + A_b e^{-Bq(t)} + Pol_{res} i_f - Cq(t) \quad (2)$$

where

- $E_0$  is the battery thermodynamics voltage (V);
- $K$  is the polarization constant (V/Ah);
- $Q_b$  is the battery maximum capacity (Ah);
- $i_f$  is the filtered battery current (A);
- $q(t)$  denotes the time integral of the extracted current (Ah), i.e.,  $q(t) = -\int_0^t i dt$ , meaning that  $Q_b - q(t)$  is the actual battery charge (Ah);
- $A_b$  is the exponential zone amplitude (V);
- $B$  is the exponential zone time constant inverse 1/(Ah);
- $C$  is the polarization voltage slope V/(Ah);
- $R$  is the battery internal resistance ( $\Omega$ );
- $Pol_{res}$  is the polarization resistance ( $\Omega$ ).

The polarization resistance changes if the battery is discharging or charging according to the next relation:

$$Pol_{res} = K \frac{Q_b}{Q_b - q(t)} (1 - u) + K \frac{Q_b}{q(t) + 0.1Q_b} u \quad (3)$$

where  $u$  is a binary variable, equal to one when  $i > 0$ , i.e., charging, and  $K$  is intended as a polarization resistance constant with the same value as the one in the second term in (2) but measured in  $\Omega$ .

Model (2) in discharging mode is valid for  $q(t) \in [0, Q_b)$ . At  $q(t) = Q_b$ , there is a vertical negative asymptote. Moreover, given a (negative) discharge current  $i_{dis}$ , we have that, at fully charged condition ( $q(t) = 0$ ):

$$V_b = E_0 + Ri_{dis} + A_b = V_{full} \quad (4)$$

where  $V_{full}$  is the fully charged voltage.

The battery maximum capacity  $Q_b$  is the maximum theoretical discharge capacity. However, batteries are operated in a range of voltage that goes from  $V_{full}$  to the cut-off voltage  $V_{cut-off}$  (V), which are parameters usually provided on the battery datasheet. Let us indicate with  $Q$  (Ah) the battery nominal capacity, which corresponds to the discharged capacity from  $V_{full}$  to  $V_{cut-off}$  at the nominal discharge current  $i_{dis}^{nom}$  (A). Figure 6 helps to make clear the difference between  $Q_b$  and  $Q$ .

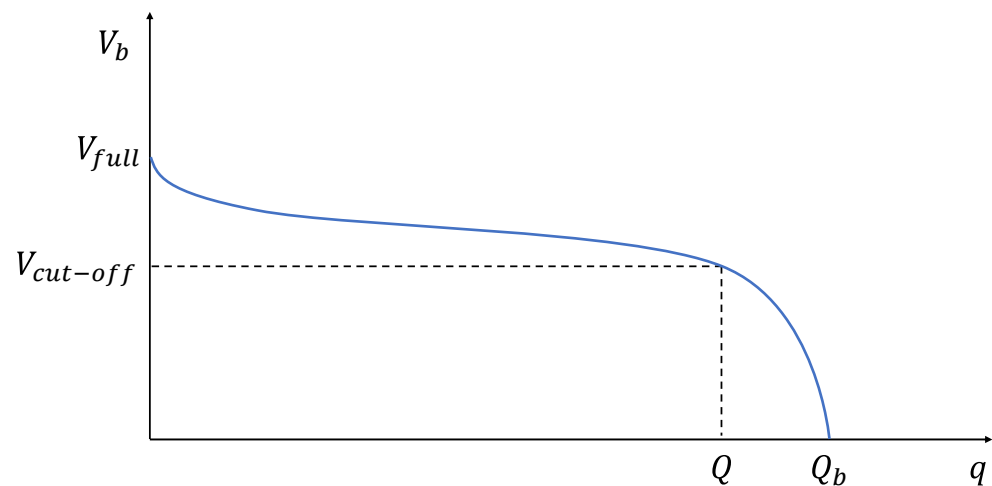


**Figure 6.** Example of discharge curve at nominal discharge current.

The battery cut-off voltage  $V_{cut-off}$  and  $Q$  are related by the following equation:

$$V_b = E_0 - K \frac{Q_b}{Q_b - Q} (Q - i_{dis}^{nom}) + Ri_{dis}^{nom} + A_b e^{-BQ} - CQ = V_{cut-off} \quad (5)$$

From (5), it is possible to find a direct relation between  $Q_b$  and  $Q$ :

$$Q_b(Q) = Q \frac{z}{z - 1} \quad (6)$$

$$z = \frac{E_0 + Ri_{dis}^{nom} + A_b e^{-BQ} - CQ - V_{cut-off}}{K(Q - i_{dis}^{nom})}$$

Note that the capacity that can be measured with an experimental full discharge cycle is actually  $Q$ ; then, the battery capacity  $Q_b$  can be computed using (6). Hereafter, we will refer to  $Q$  simply as the battery capacity. As demonstrated in Appendix A, relation (5) can also be solved with respect to  $Q$  and the relation  $Q(Q_b)$  obtained.

The filtered battery current is computed as follows:

$$i_f(t) = \mathcal{L}^{-1} \left( \frac{1}{1 + s \cdot T_d} \cdot I(s) \right) \quad (7)$$

where  $\mathcal{L}^{-1}$  is the inverse Laplace transform,  $I(s)$  is the Laplace transform of the battery current, and  $T_d(s)$  is the battery response time.

### 3.1.2. Block E1

In Block E1, to account for the impact of the battery temperature on the EM, the thermodynamics voltage  $E_0$ , the polarization constant  $K$ , the internal resistance  $R$ , and the exponential zone amplitude  $A_b$  are calculated according to Nernst and Arrhenius laws as follows [36]:

$$E_0(T) = E_0|_{T_{ref}} + \frac{\partial E}{\partial T}(T - T_{ref}) \quad (8)$$

$$K(T) = K|_{T_{ref}} \exp\left(\alpha\left(\frac{1}{T} - \frac{1}{T_{ref}}\right)\right) \quad (9)$$

$$R(T) = R|_{T_{ref}} \exp\left(\beta\left(\frac{1}{T} - \frac{1}{T_{ref}}\right)\right) \quad (10)$$

$$A_b(T) = A_b|_{T_{ref}} + \frac{\partial A_b}{\partial T}(T - T_{ref}) \quad (11)$$

where  $T$  (K) is the battery temperature,  $T_{ref}$  (K) is the reference battery temperature,  $\partial E/\partial T$  is the open circuit temperature coefficient (V/K),  $\alpha$  and  $\beta$  are the Arrhenius constants for the polarization resistance and internal resistance, respectively, and  $\partial A_b/\partial T$  is a parameter that models the linear dependence of the exponential zone amplitude from the temperature. In the literature, it is common to find battery models such as the one in (2); however, none of them considers a temperature dependence of the parameter  $A_b$ . The choice of modeling the exponential zone amplitude  $A_b$  as a temperature-linear function was made by carefully looking at the experimental results. This alternative turned out to outperform the option in which  $A_b$  is constant. In Block E2 the impact of the battery temperature on the battery maximum capacity at BoL  $Q_b^{BoL}$  is also accounted for as follows:

$$Q_b^{BoL}(T) = Q_b|_{T_{ref}} + \frac{\Delta Q_b}{\Delta T}(T - T_{ref}) \quad (12)$$

where  $\Delta Q_b/\Delta T$  is the battery capacity temperature coefficient (Ah/K).

### 3.2. Battery Aging Model

The battery AM modifies the battery capacity  $Q_b$  and resistance  $R$  based on ongoing aging and consists of four main blocks:

1. Block A1, which determines the DoD, and average C-rates and battery temperature during each cycle;
2. Block A2, which evaluates the battery stress arising during any cycle in the function of DoD, C-rates, and temperature;
3. Block A3, which computes the aging index  $\varepsilon$ , based on the concept of equivalent number of cycles;
4. Block A4, which adjusts the battery capacity and resistance according to the actual value of the aging index.

The interconnections among these four blocks are highlighted in Figure 7, which shows the detailed WBM scheme.

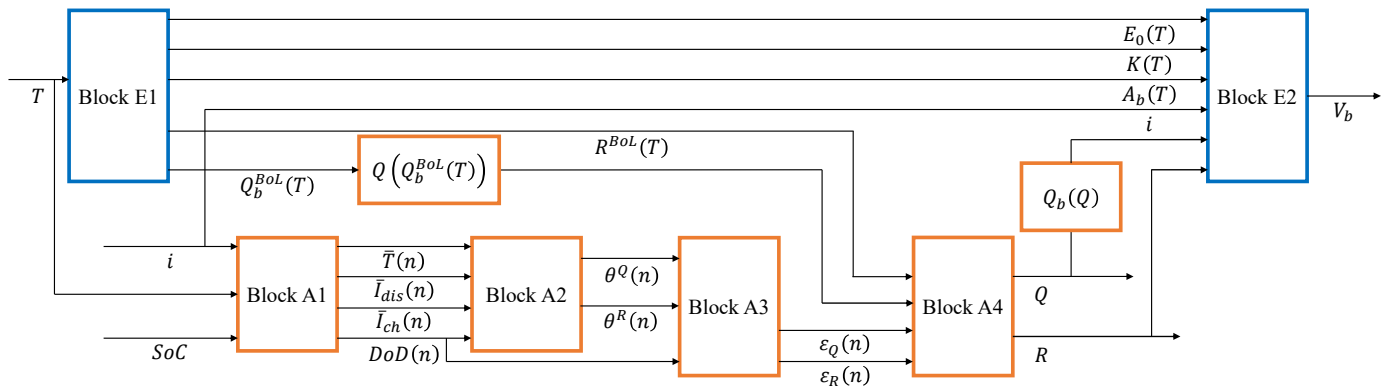


**Figure 7.** Detailed block scheme of the WBM (exploded version of Figure 5). Blue blocks compose the electrothermal model; orange blocks compose the aging model.

### 3.2.1. Block A1

Block A1 works on a discrete time base, assuming that  $SoC(k)$  and  $i(k)$  are the measures of SOC (p.u.) and battery current at the discrete time step  $k \cdot \Delta t$ ,  $k = 1, 2, \dots$ . Using these measurements, Block A1 updates the DoD, the average C-rates  $\bar{I}_{dis}$  and  $\bar{I}_{ch}$  during discharge and charge, respectively, and the average battery temperature  $\bar{T}$ , when the battery transits from charge to discharge or vice versa. These updates are therefore indexed by the transition number  $n$ . A new transition is detected by monitoring the change in sign of the variation of the SOC defined as

$$\Delta SoC(k) = SoC(k) - SoC(k-1) \quad (13)$$

Therefore, the update of the DoD and the average C-rates and battery temperature is carried out by executing Algorithm 1.

---

**Algorithm 1** DoD, C-rates and battery temperature update.

---

1. initialize the transition number,  $n = 1$ , the DoD,  $DoD(1) = 1 - SoC_{init}$ , where  $SoC_{init}$  is the battery initial SOC, the C-rates,  $\bar{I}_{dis}(1) = i_{init}$ ,  $\bar{I}_{ch}(1) = i_{init}$ , where  $i_{init}$  is the battery initial current, and the previous transition time step  $k_p = 0$ ;
  2. at every time step  $k$ ,
  3. evaluate  $\Delta SoC(k)$  as in (13);
  4. **if**  $\Delta SoC(k) \cdot \Delta SoC(k-1) < 0$ :
  5.      $n = n+1$ ;
  6.     calculate DoD as  $DoD(n) = 1 - SoC(k-1)$ ;
  7.     calculate  $\bar{I}_{dis}(n)$  and  $\bar{I}_{ch}(n)$  using (14) and (15);
  8.     calculate  $\bar{T}(n)$  using (16);
  9.      $k_p = k$ ;
  10. **end if**
- 

$$\bar{I}_{dis}(n) = \begin{cases} \frac{1}{k-k_p} \sum_{j=k_p}^{k-1} |i(j)| & \Delta SoC(k) > 0 \\ \bar{I}_{dis}(n-1), & \Delta SoC(k) \leq 0 \end{cases} \quad (14)$$

$$\bar{I}_{ch}(n) = \begin{cases} \bar{I}_{ch}(n-1), & \Delta SoC(k) > 0 \\ \frac{1}{k-k_p} \sum_{j=k_p}^{k-1} |i(j)|, & \Delta SoC(k) \leq 0 \end{cases} \quad (15)$$

$$\bar{T}(n) = \frac{1}{k-k_p} \sum_{j=k_p}^{k-1} T(j) \quad (16)$$

### 3.2.2. Block A2

In Block A2, the battery stress factor at transition  $n$  is computed. This factor must measure the degradation of the battery due to its use between transition  $n - 1$  and transition  $n$ . Such a battery use is characterized by the DoD, the average C-rates, and the average temperature, computed by Block A1, which influence the battery stress as modeled in the following.

The stress factor  $\theta_T$  due to temperature is computed using the Arrhenius equation:

$$\theta_T(n) = \exp \left[ -\psi \left( \frac{1}{\bar{T}(n)} - \frac{1}{T_{ref}} \right) \right] \quad (17)$$

where  $T_{ref}$  is the model reference temperature and  $\psi$  is the Arrhenius rate constant. By analogy with Miner's rule, using Wöhler approximation, the stress factors associated with the discharge and charge currents are computed as follows:

$$\theta_{I_{dis}}(n) = \left( \frac{\bar{I}_{dis}(n)}{I_{dis}^{ref}} \right)^{1/\gamma_d} \quad (18)$$

$$\theta_{I_{ch}}(n) = \left( \frac{\bar{I}_{ch}(n)}{I_{ch}^{ref}} \right)^{1/\gamma_c} \quad (19)$$

where  $I_{dis}^{ref}$  and  $I_{ch}^{ref}$  are the peak stress amplitudes for the discharge and charge current, respectively, and both are positive;  $\gamma_d$  and  $\gamma_c$  are the stress exponents for the discharge and charge current, respectively.

Similarly, the stress factor  $\theta_{DoD}$  associated with a given DoD can be computed as follows:

$$\theta_{DoD}(n) = (DoD(n))^{1/\xi} \quad (20)$$

where  $\xi$  is the stress exponent for the DoD.

The final combined stress factor is given by

$$\theta(n) = \theta_{DoD}(n) \cdot \theta_{I_{dis}}(n) \cdot \theta_{I_{ch}}(n) \cdot \theta_T(n) \quad (21)$$

Based on the experimental results, the accuracy of the overall AM drops if the same stress factor is used for both capacity and resistance, as usually carried out in literature papers such as [20]. Therefore, in this paper, we define two different stress factors  $\theta^Q(n)$  and  $\theta^R(n)$  for capacity and resistance, respectively. This means that the relations in (17)–(21) must be considered as defined twice, one for capacity and one for resistance. In particular:

- $\theta^Q(n)$  is obtained by applying (21) starting from (17)–(20) with  $\psi = \psi_Q$ ,  $\gamma_d = \gamma_{dQ}$ ,  $\gamma_c = \gamma_{cQ}$ , and  $\xi = \xi_Q$ ;
- $\theta^R(n)$  is obtained by applying (21) starting from (17)–(20) with  $\psi = \psi_R$ ,  $\gamma_d = \gamma_{dR}$ ,  $\gamma_c = \gamma_{cR}$ , and  $\xi = \xi_R$ .

### 3.2.3. Block A3

Block A3 computes the aging index  $\varepsilon(n)$ . Such an index represents the contribution of the battery use between transition  $n - 1$  and transition  $n$  to the total aging of the battery.

Let us define first  $N_c^{ref}$  as the number of cycles from BoL to EoL in reference use conditions, i.e., when the battery use is with DoD = 1 and with reference C-rates and battery temperature. Under reference conditions, the aging index after one cycle (two transitions) is given by

$$\varepsilon = \frac{1}{N_c^{ref}} \quad (22)$$

Knowing that, in real load profiles, charging and discharging cycles do not always cover the entire battery capacity ( $\text{DoD} < 1$ ), the equivalent number of full cycles  $N_{eq}$  is computed at each transition  $n$  as follows:

$$N_{eq}(n) = \begin{cases} 1 - \frac{\text{DoD}(n-2) + \text{DoD}(n)}{2\text{DoD}(n-1)}, & \Delta \text{SoC}(k) > 0 \\ 0, & \text{otherwise} \end{cases} \quad (23)$$

Then, given  $N_{eq}(n)$ , the aging index  $\varepsilon(n)$  is updated as follows:

$$\varepsilon(n) = \varepsilon(n-1) + \frac{N_{eq}(n)}{N_c^{ref}} \theta(n-1) \quad (24)$$

Since we have two different stress factors for capacity and resistance, we also have two different aging indices  $\varepsilon_Q(n)$  and  $\varepsilon_R(n)$  computed by applying (24) with  $\theta^Q(n)$  and  $\theta^R(n)$ , respectively.

### 3.2.4. Block A4

Finally, in Block A4, the battery capacity and internal resistance are updated based on ongoing degradation through the computation of the aging index  $\varepsilon_{Q/R}$ . In particular, the maximum capacity  $Q$  and the internal resistance  $R$  are expressed as

$$Q(n) = Q_{BoL} - \varepsilon_Q(n)^{\lambda_Q} \cdot (Q_{BoL} - Q_{EoL}) \quad (25)$$

$$R(n) = R_{BoL} + \varepsilon_R(n)^{\lambda_R} \cdot (R_{EoL} - R_{BoL}) \quad (26)$$

where

- $Q_{BoL}$  and  $Q_{EoL}$  are the battery capacity (Ah) at BoL and EoL, respectively;
- $R_{BoL}$  and  $R_{EoL}$  are the battery resistance ( $\Omega$ ) at BoL and EoL, respectively;
- $\lambda_Q$  and  $\lambda_R$  are the aging exponents for the battery maximum capacity and internal resistance, respectively.

### 3.3. Novelty Aspects

We remark that the battery models introduced in this section build upon existing electrothermal and aging Li-ion cell models. Specifically, the EM is formulated based on the models in [11,24,25], while the AM originates from the framework presented in [20]. However, in this paper, we formalize the integration of the EM and the AM, depicted in Figure 7, by including the relation between the maximum theoretical discharge capacity  $Q_b$  and the battery nominal capacity  $Q$ . Indeed, in [20], this relation is not explicitly taken into account. Moreover, differently from [20] and from other literature approaches, in this paper we differentiate the computation of the aging index for capacity and resistance.

## 4. Parameter Identification

In this section, the method to estimate the EM and AM parameters is presented.

### 4.1. Battery Electrothermal Model Parameter Identification

Based on the experimental data set described in Section 2.1.1, we assume to be provided with the measurements of the trajectories of the battery output voltage during a series of discharges at a constant rate and at  $r$  different temperatures  $T = T_1, T_2, \dots, T_r$ , denoted as  $\{V^T(t)\}_{T=T_1}^{T_r}$ .

The proposed identification procedure consists of three steps, detailed in the flowchart in Figure 8, and it was developed to cope with the complexity of battery voltage representation (2).



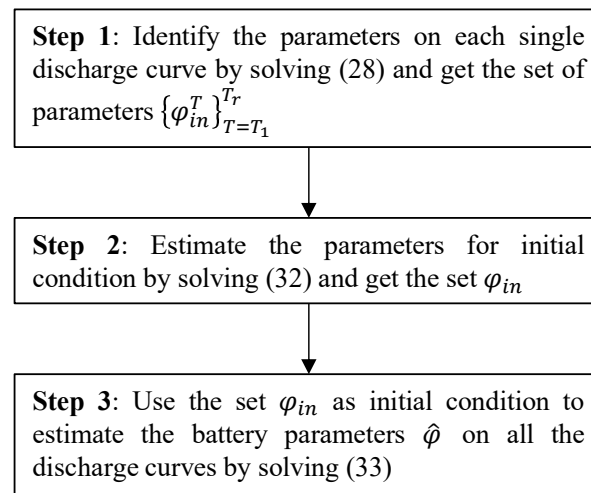


**Figure 8.** Flowchart of the battery electrothermal model parameter identification algorithm.

Let us indicate with  $\varphi$  a vector composed of the 12 EM parameters:

$$\varphi = [E_0|_{T_{ref}}, \partial E / \partial T, K|_{T_{ref}}, \alpha, R|_{T_{ref}}, \beta, Q|_{T_{ref}}, \Delta Q / \Delta T, A_b|_{T_{ref}}, \partial A_b / \partial T, B, C] \quad (27)$$

The idea is to first identify a collection of  $r$  temperature-dependent estimates  $\{\varphi_{in}^T\}_{T=T_1}^{T_r}$  of the vector  $\varphi$ , one from each voltage trajectory  $\{V^T(t)\}_{T=T_1}^{T_r}$  (Step 1). Then, these estimates are used to define a single initial estimate  $\varphi_{in}$ , independent of the temperature, by adopting a fitting procedure on suitably defined functions (Step 2). Finally,  $\varphi_{in}$  is used as the initial conditions to compute the final estimate  $\hat{\varphi}$  using least-square minimization (Step 3). The details of each step of the identification algorithm are given in the following.

#### 4.1.1. Step 1

Given one of the voltage trajectories  $V^T(t)$  the temperature-dependent estimate  $\varphi_{in}^T$  is computed by solving the following problem:

$$\varphi_{in}^T = \arg \min_{\varphi} \sum_{t=0}^{EoD} \left( \frac{V^T(t) - V_b^{\varphi}(t, T)}{V^T(t)} \right)^2 \quad (28)$$

where  $EoD$  is the time duration of the discharge, and  $V_b^{\varphi}(t, T)$  is given by (2) with  $E_0 = E_0(T)$ ,  $R = R(T)$ ,  $K = K(T)$ ,  $Q_b = Q_b(T)$ ,  $A_b = A_b(T)$ , according to (8)–(12), and given a value for the set of parameters in  $\varphi$ . We remark that, in solving (28), the following initial conditions for  $A_b|_{T_{ref}}$ ,  $B$ , and  $C$  can be used [11,25]:

$$A_b|_{T_{ref}} = V_{full} - V_{exp} \quad (29)$$

$$B = \frac{3}{Q_{exp}} \quad (30)$$

$$C = \frac{V_{11} - V_{12}}{Q_{12} - Q_{11}} \quad (31)$$

where  $V_{exp}$  is the voltage at the end of the exponential zone in the battery discharge profile;  $Q_{exp}$  is the charge extracted from  $V_{full}$  to  $V_{exp}$ ;  $V_{11}$  and  $V_{12}$  are the voltages at the end of the exponential zone and at the end of the linear zone when the battery is discharged at 25 °C; and  $Q_{11}$  and  $Q_{12}$  are the extracted charges from  $V_{full}$  to  $V_{11}$  and from  $V_{full}$  to  $V_{12}$ , respectively, at 25 °C.

#### 4.1.2. Step 2

The collection  $\{\varphi_{in}^T\}_{T=T_1}^{T_r}$  is used to define the unique initial condition  $\varphi_{in}$  for the final battery parameter identification. This is carried out by solving the following least-square problems:

$$\{\varphi_{in}\}_{\kappa} = \operatorname{argmin}_{\{\varphi\}_{\kappa}} \sum_T \left( g_{\kappa}^T \left( \{\varphi_{in}\}_{\kappa} \right) - g_{\kappa}^T(\{\varphi\}_{\kappa}) \right)^2 \quad (32)$$

where  $g_{\kappa}^T(\cdot)$  is a function involving the battery parameters and the battery temperature. The subscript  $\kappa$  determines the form of the function. Each  $g_{\kappa}^T(\cdot)$  involves the subset  $\{\varphi\}_{\kappa}$  of the battery parameters. For example, for  $\kappa = 1$ ,  $g_{\kappa}^T$  is given by (8) and the involved parameters are  $\{\varphi\}_{\kappa} = \{E_0|_{T_{ref}}, \partial E/\partial T\}$ . The other expressions for  $g_{\kappa}^T$  are given by the second members of (9)–(12) for parameters  $K|_{T_{ref}}, \alpha, R|_{T_{ref}}, \beta, Q|_{T_{ref}}, \Delta Q/\Delta T, A_b|_{T_{ref}}$ , and  $\partial A_b/\partial T$ . For parameters  $B$  and  $C$ ,  $g_{\kappa}$  is a constant function (so that average values are computed by (32)). The formal definition of function  $g_{\kappa}^T$  is given in Appendix B.

#### 4.1.3. Step 3

The parameter set  $\varphi_{in}$  is used as initial condition to compute the estimate  $\hat{\varphi}$  for the parameter set  $\varphi$  by solving the following least-square problem:

$$\hat{\varphi} = \operatorname{argmin}_{\varphi} \sum_{T=T_1}^{T_r} \sum_{t=0}^{EoD} \left( \frac{V^T(t) - V_b^{\varphi}(t, T)}{V^T(t)} \right)^2 \quad (33)$$

that considers the entire dataset all at once.

### 4.2. Battery Aging Model Parameter Identification

To identify the parameters of the AM, we use the data from Experiment 2, described in Section 2.1.2. We first identify the parameters directly involved in (25) and (26). Then, we identify the parameters required to compute the aging indices  $\varepsilon_Q(n)$  and  $\varepsilon_R(n)$ .

Let us consider first that, if we realize full cycles at reference conditions,  $\theta^Q(n) = \theta^R(n) = 1$  when  $n$  is even and  $\theta^Q(n) = \theta^R(n) = 0$  otherwise (according to (17)–(21)),  $N_{eq}(n) = 1$  if  $n$  is odd and  $N_{eq}(n) = 0$  otherwise (according to (23)). Therefore, from (24), it follows that  $\varepsilon_Q(n) = \varepsilon_R(n) = \lfloor n/2 \rfloor / N_c^{ref}$ , where  $\lfloor \cdot \rfloor$  indicates the integer floor part of a given number. We also remark that  $\lfloor n/2 \rfloor$  is equal to the realized full cycles  $N$ . Therefore, under the conditions of Experiment 2 cycle test #1, which are the reference ones (see Table 1), (25) and (26) can be rewritten as follows:

$$Q(N) = Q_{BoL} - N^{\lambda_Q} \nu_Q \quad (34)$$

$$R(N) = R_{BoL} + N^{\lambda_R} \nu_R \quad (35)$$

According to the description of Experiment 2 cycle test #1 in Section 2.1.2, we can generally assume to be provided with  $S$  experimental points  $(N_i, Q_i)$  and  $(N_i, R_i)$ ,  $i = 1, 2, \dots, S$ . Therefore, the parameters in (34) and (35) can be computed by fitting the experimental results through least-square minimization:

$$\lambda_Q, Q_{BoL}, \nu_Q = \operatorname{argmin} \sum_{i=1}^S \left( Q_i - \tilde{Q}_{BoL} + N_i^{\tilde{\lambda}_Q} \tilde{\nu}_Q \right)^2 \quad (36)$$

$$\lambda_R, R_{BoL}, \nu_R = \operatorname{argmin} \sum_{i=1}^S \left( R_i - \tilde{R}_{BoL} - N_i^{\tilde{\lambda}_R} \tilde{\nu}_R \right)^2 \quad (37)$$

and, then, considering that  $Q_{EoL} = 0.8 \cdot Q_{BoL}$ , it is possible to compute  $N_c^{ref}$  and  $R_{EoL}$  as follows:

$$N_c^{ref} = \left( \frac{0.2 \cdot Q_{BoL}}{\nu_Q} \right)^{1/\lambda_Q} \quad (38)$$

$$R_{EoL} = \nu_R (N_c^{ref})^{\lambda_R} + R_{BoL}. \quad (39)$$

In the case we are provided with known and unique values for the BoL capacity and resistance  $Q_{BoL}$  and  $R_{BoL}$ , the fitting curves must be forced to start from these two values, by applying (36) and (37) without considering  $\tilde{Q}_{BoL}$  and  $\tilde{R}_{BoL}$  as optimization variables. In the results presented in this paper, we applied this case.

Once the parameters  $\lambda_Q$ ,  $\lambda_R$ ,  $Q_{BoL}$ ,  $R_{BoL}$ ,  $Q_{EoL}$ ,  $R_{EoL}$ , and  $N_c^{ref}$  are identified using the experimental results from Experiment 2 cycle test #1, the parameters required to compute  $\varepsilon_Q(n)$  and  $\varepsilon_R(n)$  have to be identified. More specifically, we need to estimate the following vector:

$$\varphi_a = [\psi_Q, \gamma_{dQ}, \gamma_{cQ}, \xi_Q, \psi_R, \gamma_{dR}, \gamma_{cR}, \xi_R] \quad (40)$$

To this end, we can use the experimental results from Experiment 2 cycle tests #2, #3, #4, and #6. As for cycle test #1, we have that  $N_{eq}(n) = 1$  when  $n$  is odd and  $N_{eq}(n) = 0$  otherwise. Consider now that cycle tests #2, #3, #4, and #6 do not adopt reference values just for temperature, charge and discharge rate, and DoD, respectively, as highlighted in Table 1. Therefore, assuming that  $T_2$  is the battery temperature in cycle test #2,  $I_{ch,3}$  is the charging current in cycle test #3, and  $I_{dis,4}$  is the discharging current in cycle test #4, we have the following:

- For Experiment 2 cycle test #2:

$$\theta^{Q/R}(n) = \theta_{DoD}^{Q/R}(n) \theta_T^{Q/R}(n) = e^{-\psi_{Q/R} \cdot \left( \frac{1}{T_2} - \frac{1}{T_{ref}} \right)} \quad (41)$$

when  $n$  is even and  $\theta^{Q/R}(n) = 0$  otherwise;

- For Experiment 2 cycle test #3:

$$\theta^{Q/R}(n) = \theta_{DoD}^{Q/R}(n) \theta_{ch}^{Q/R}(n) = \left( \frac{I_{ch,3}}{I_{ch}^{ref}} \right)^{\frac{1}{\gamma_{cQ/R}}} \quad (42)$$

when  $n$  is even and  $\theta^{Q/R}(n) = 0$  otherwise;

- For Experiment 2 cycle test #4:

$$\theta^{Q/R}(n) = \theta_{DoD}^{Q/R}(n) \theta_{dis}^{Q/R}(n) = \left( \frac{I_{dis,4}}{I_{dis}^{ref}} \right)^{\frac{1}{\gamma_{dQ/R}}} \quad (43)$$

when  $n$  is even and  $\theta^{Q/R}(n) = 0$  otherwise;

- For Experiment 2 cycle test #6:

$$\theta^{Q/R}(n) = \theta_{DoD}^{Q/R}(n) = (0.8)^{\frac{1}{\xi_{Q/R}}} \quad (44)$$

when  $n$  is even and  $\theta^{Q/R}(n) = 0$  otherwise.

Using (41)–(44) and assuming that  $N = \lfloor n/2 \rfloor$  is the number of realized (not necessarily full) cycles at transition  $n$ , from (24), we can compute the aging index  $\varepsilon_{Q/R}^j$  referring to cycle test  $j = 2, 3, 4, 6$  as a function of  $N$  and of the relevant aging parameter as follows:

- For Experiment 2 cycle test #2:

$$\varepsilon_{Q/R}^2(N, \psi_{Q/R}) = \frac{N}{N_c^{ref}} \cdot e^{-\psi_{Q/R} \cdot \left( \frac{1}{T_2} - \frac{1}{T_{ref}} \right)} \quad (45)$$

- For Experiment 2 cycle test #3:

$$\varepsilon_{Q/R}^3(N, \gamma_{cQ/R}) = \frac{N}{N_c^{ref}} \cdot \left( \frac{I_{ch,3}}{I_{ch}^{ref}} \right)^{\frac{1}{\gamma_{cQ/R}}} \quad (46)$$

- For Experiment 2 cycle test #4:

$$\varepsilon_{Q/R}^4(N, \gamma_{dQ/R}) = \frac{N}{N_c^{ref}} \cdot \left( \frac{I_{dis,4}}{I_{dis}^{ref}} \right)^{\frac{1}{\gamma_{dQ/R}}} \quad (47)$$

- For Experiment 2 cycle test #6:

$$\varepsilon_{Q/R}^6(N, \zeta_{Q/R}) = \frac{N}{N_c^{ref}} \cdot (0.8)^{\frac{1}{\zeta_{Q/R}}} \quad (48)$$

By applying (45)–(48) to (25)–(26), we can also compute the aging expressions for capacity and resistance referring to cycle tests  $\#i$ ,  $i = 2, 3, 4, 6$  as a function of  $N$  and the relevant aging parameter,  $Q^i(N, \cdot)$  and  $R^i(N, \cdot)$ .

According to the description of Experiment 2 in Section 2.1.2, we can generally assume to be provided with  $S_j$  experimental points  $(N_i^j, Q_i^j)$  and  $(N_i^j, R_i^j)$ ,  $i = 1, 2, \dots, S_j$ ,  $j = 2, 3, 4, 6$ . Therefore, the parameters in (40) can be identified by fitting the experimental results through least-square minimization:

$$\psi_Q = \arg \min_{\tilde{\psi}_Q} \sum_{i=1}^{S_2} \left( Q_i^2 - Q^2(N_i^2, \tilde{\psi}_Q) \right)^2 \quad (49)$$

$$\psi_R = \arg \min_{\tilde{\psi}_R} \sum_{i=1}^{S_2} \left( R_i^2 - R^2(N_i^2, \tilde{\psi}_R) \right)^2 \quad (50)$$

$$\gamma_{cQ} = \arg \min_{\tilde{\gamma}_{cQ}} \sum_{i=1}^{S_3} \left( Q_i^3 - Q^3(N_i^3, \tilde{\gamma}_{cQ}) \right)^2 \quad (51)$$

$$\gamma_{cR} = \arg \min_{\tilde{\gamma}_{cR}} \sum_{i=1}^{S_3} \left( R_i^3 - R^3(N_i^3, \tilde{\gamma}_{cR}) \right)^2 \quad (52)$$

$$\gamma_{dQ} = \arg \min_{\tilde{\gamma}_{dQ}} \sum_{i=1}^{S_4} \left( Q_i^4 - Q^4(N_i^4, \tilde{\gamma}_{dQ}) \right)^2 \quad (53)$$

$$\gamma_{dR} = \arg \min_{\tilde{\gamma}_{dR}} \sum_{i=1}^{S_4} \left( R_i^4 - R^4(N_i^4, \tilde{\gamma}_{dR}) \right)^2 \quad (54)$$

$$\zeta_Q = \arg \min_{\tilde{\zeta}_Q} \sum_{i=1}^{S_6} \left( Q_i^6 - Q^6(N_i^6, \tilde{\zeta}_Q) \right)^2 \quad (55)$$

$$\zeta_R = \arg \min_{\tilde{\zeta}_R} \sum_{i=1}^{S_6} \left( R_i^6 - R^6(N_i^6, \tilde{\zeta}_R) \right)^2 \quad (56)$$

#### 4.3. Novelty Aspects

We remark that the aging parameter identification procedure introduced in Section 4.2 builds upon the procedure presented in [20]. However, in [20], the identification process requires the use of just six experimental points (couples composed of the number of cycles and capacity measurements  $(N_i, Q_i)$ ), at specific capacity fade conditions: loss of 5% to get five experimental points and loss of 20% to get the sixth point (see Figure 5 in [20]).

However, to obtain these specific points, very frequent capacity measurements should be carried out in order to exactly establish the number of cycles at which the 5% and

20% capacity fade occur. Therefore, we considered the following: (1) performing frequent enough capacity measurements to identify exactly when the 5% and 20% decreases occur was impractical since, according to the description provided in Section 2.1.1, an accurate capacity measurement requires two hours; and (2) if more than six capacity measurements are available, they should be used in the identification process to achieve higher robustness against measurement errors.

Therefore, we decided the following: (1) to carry out an easier and more linear measurement process where capacity (and resistance) measurements are acquired at regular cycle intervals, as described in Section 2.1.2 (Experiment 2); and (2) to generalize the identification procedure in [20] allowing the use of a general set of experimental points, not necessarily at specific capacity fade levels and as numerous as possible, to increase robustness with respect to measurement errors.

## 5. Results

In the following, the results of the parameter identification and validation of the WBM are presented. The applied identification methodologies are the one detailed in Section 4.1 for the EM parameters and the one detailed in Section 4.2 for the AM parameters. The parameters of the WBM are also cross-validated on discharge curves at different aging levels of the cells, as the results of the identification of the AM parameters directly influence the battery voltage during the operations.

Furthermore, two sensitivity analyses are performed on the identification of the WBM parameters. In the first one, we explored the impact of varying the sampling time  $\delta$  (s) for the measurements in the discharge curves of Experiment 1. Three different sampling times were considered:  $\delta = 1, 5, 10$  s. In the second sensitivity analysis, we investigated the influence of the number of capacity and resistance measurements available from Experiment 2. In this analysis, we indicate as Case 1 the scenario where all the capacity and resistance measurements are used to estimate the AM parameters, and as Case 2 the scenario where only half of the capacity and resistance measurements from Experiment 2 are employed, with one measurement employed for every two available.

### 5.1. Error Metrics

In the following, result performances will be analyzed in terms of maximum Absolute Percentage Error (maxAPE) and Mean Absolute Percentage Error (MAPE). We first define the APE for battery voltage, capacity, and resistance as follows

$$APE_V(t) = \left| \frac{V_b(t) - \hat{V}_b(t)}{V_{nom}} \right| 100\%, \quad t \in [0, EoD] \quad (57)$$

$$APE_{SoH}(i) = \left| \frac{Q_i - \hat{Q}_i}{Q_{BoL}} \right| 100\%, \quad i = 1, 2, \dots, S \quad (58)$$

$$APE_R(i) = \left| \frac{R_i - \hat{R}_i}{R_{BoL}} \right| 100\%, \quad i = 1, 2, \dots, S \quad (59)$$

where  $V_b(t)$  and  $\hat{V}_b(t)$  are the battery voltages at time  $t$  measured and reproduced by the identified model, respectively;  $Q_i$ ,  $R_i$ ,  $\hat{Q}_i$ , and  $\hat{R}_i$  are the measured and estimated battery capacity and resistance, respectively, at the  $i$ -th measurement within a set of cardinality  $S$ .

Therefore,  $MAPE_x$  and  $maxAPE_x$ , with  $x = V, SoH, R$ , are defined as follows:

$$MAPE_V = \frac{1}{EoD + 1} \sum_{t=0}^{EoD} APE_V(t) \quad (60)$$

$$maxMAPE_V = \max_{t \in [0, EoD]} APE_V(t) \quad (61)$$

$$MAPE_Q = \frac{1}{S} \sum_{i=1}^S APE_Q(i) \quad (62)$$

$$\max MAPE_Q = \max_{i \in [1, S]} APE_Q(i) \quad (63)$$

$$MAPE_R = \frac{1}{S} \sum_{i=1}^S APE_R(i) \quad (64)$$

$$\max MAPE_R = \max_{i \in [1, S]} APE_R(i) \quad (65)$$

## 5.2. Battery Electrothermal Model Parameters

The parameters of the EM were identified applying the methodology presented in Section 4.1 to the experimental results of Experiment 1. After being identified, the EM parameters were validated using the discharge curves of Experiment 3. All measurements collected in Experiment 1 and Experiment 3 have a sampling time of 1 s. However, the identification procedure has been applied using three different sampling time values, namely,  $\delta = 1, 5, 10$  s, in order to analyze the performance of our approach with a sampling time larger than 1 s.

Table 2 shows the values of the identified parameters at the three investigated sampling times. The results of the identification in terms of  $MAPE_V$  and  $\max APE_V$  are listed in Table 3, while Table 4 shows the results of the validation of the battery EM parameters on the discharge curves of the fresh battery, evaluated on the same metrics.

The implemented methodology is not sensible to measurement sampling times in the interval 1–10 s; indeed, the obtained error metrics are very close, both for identification (Table 3) and validation (Table 4). The temperature returning the lowest errors is 25 °C and the farther from it the larger the error. However, at every tested temperature, the voltage is well approximated, showing the effectiveness of the proposed methodology. The MAPE on the voltage is always well below 0.7% and the maxAPE is almost always below 5%. Figure 9 shows the measured and reproduced voltage profiles obtained in the case with  $\delta = 1$  s. Here, we can observe that the largest errors are in the proximity of  $V_{cut-off}$ . The validation results in the case of  $\delta = 5, 10$  s are not shown graphically as they are very similar to those of Figure 9, as expected from Table 4. Even in these cases, the largest errors are in the proximity of  $V_{cut-off}$ .

**Table 2.** Estimated values of the battery EM parameters.

$\delta$ (s)	$E_0  _{T_{ref}}$	$\frac{\partial E}{\partial T}$	$K  _{T_{ref}}$	$\alpha$	$R  _{T_{ref}}$	$\beta$	$A_b  _{T_{ref}}$	$\frac{\partial A_b}{\partial T}$	$Q_b  _{T_{ref}}$	$\frac{\Delta Q_b}{\Delta T}$	$B$	$C$	$T_d$
1	4.1261	0.0014	0.0037	−2767	0.0260	3.470	0.0414	−0.0015	4.6919	0.0165	2.9660	0.1621	67.50
5	4.1268	0.0014	0.0037	−2770	0.0262	3.465	0.0412	−0.0015	4.6913	0.0165	3.0178	0.1623	67.50
10	4.1275	0.0014	0.0037	−2768	0.0263	3.459	0.0405	−0.0015	4.6911	0.0165	3.0709	0.1624	67.50

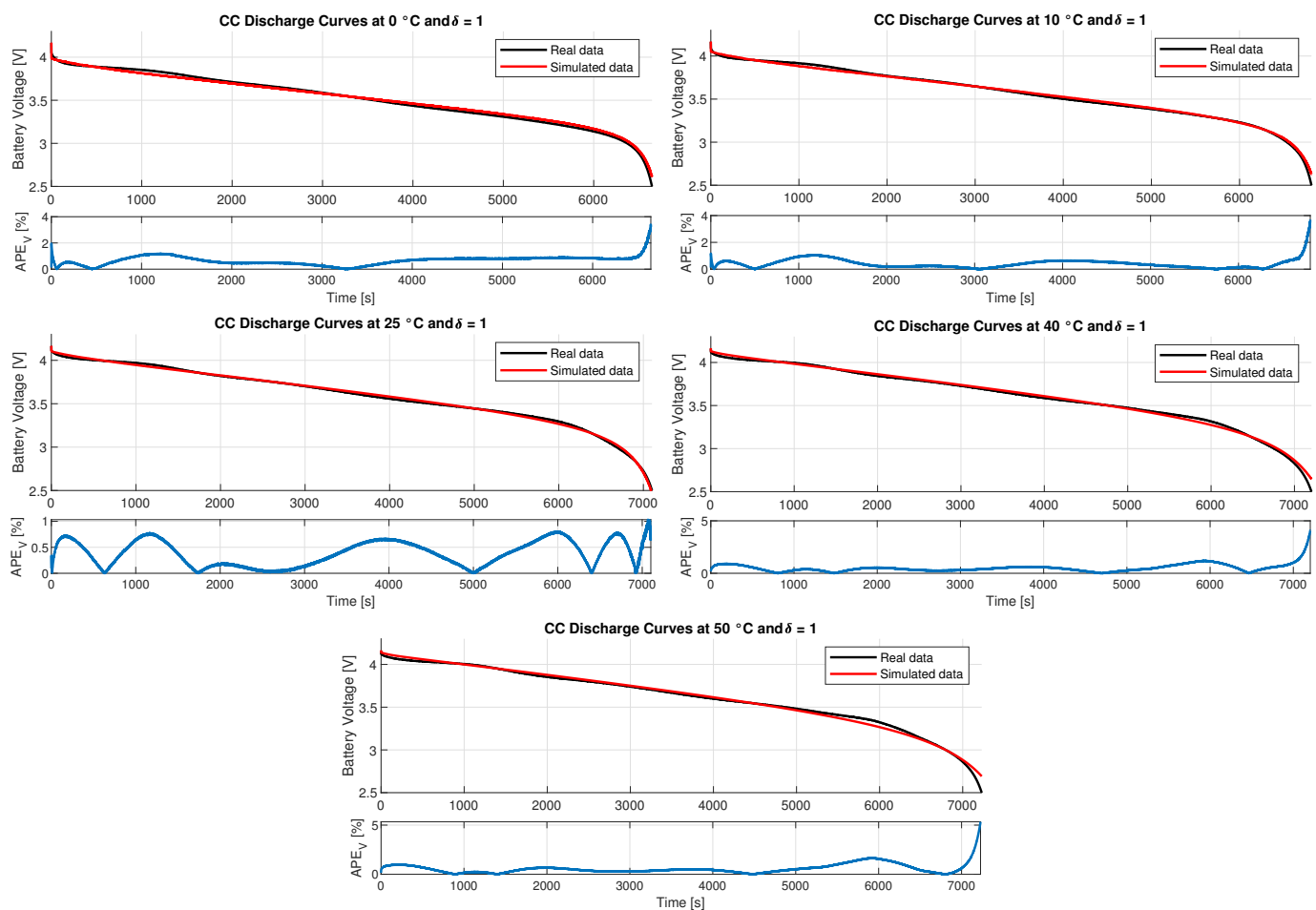
**Table 3.** Results of the identification of the battery EM.

Temperature (°C)	$\delta = 1$ s		$\delta = 5$ s		$\delta = 10$ s	
	$MAPE_V$ (%)	$\max APE_V$ (%)	$MAPE_V$ %	$\max APE_V$ (%)	$MAPE_V$ (%)	$\max APE_V$ (%)
0	0.521	1.920	0.521	1.920	0.520	1.944
25	0.390	2.094	0.391	2.097	0.391	2.104
50	0.608	5.487	0.609	5.492	0.610	5.498



**Table 4.** Results of the validation of the battery EM parameters on fresh battery discharge curves at 0.5C rate, and at 0, 25, 40, and 50 °C.

Temperature (°C)	$\delta = 1$ s		$\delta = 5$ s		$\delta = 10$ s	
	$MAPE_V$ (%)	$\max APE_V$ (%)	$MAPE_V$ (%)	$\max APE_V$ (%)	$MAPE_V$ (%)	$\max APE_V$ (%)
0	0.660	3.402	0.660	3.208	0.657	2.955
10	0.406	3.696	0.405	3.498	0.403	3.326
25	0.383	1.032	0.384	0.969	0.384	0.950
40	0.507	4.070	0.507	3.929	0.509	3.932
50	0.578	5.335	0.578	5.127	0.577	4.895

**Figure 9.** Results of the battery EM validation with a sampling time of 1 s on fresh battery discharge curves at 0.5C rate, and at 0, 25, 40, and 50 °C: voltage profiles (top figures) and  $APE_V$  (bottom figures).

The cross-validation results of the battery EM parameters on the discharge curves of the two Pattern A tests, Pattern B test, and cycle tests #1-3, #2-3, and Append 5 are shown in Table 5. The parameters are validated on the discharge curves of these tests at three different levels of battery aging:

1. Pattern A, 25 °C, at BoL, at cycle #28 and at cycle #78;
2. Pattern A, 0 °C, at BoL, at cycle #39 and at cycle #75;
3. Pattern B, at BoL, at cycle #42 and at cycle #104;
4. Cycle test #1-3, at BoL, at cycle #200 and at cycle #450;
5. Cycle test #2-3, at BoL, at cycle #200 and at cycle #450;
6. Cycle test Append 5, at BoL, at cycle #284 and at cycle #654.

In Table 5, the column titled “BoL” shows the results of the discharge curves performed at BoL, the column titled “Mid” shows the results of the discharge curves performed at the second level of battery aging, and the column titled “Last” shows the results of the discharge curves performed at the third level of battery aging. The very low MAPEs obtained on these tests prove the effectiveness of the proposed methodology and of the integration of the EM with the AM. Furthermore, the good approximation of the battery aged voltage also indicates the effectiveness of the AM parameter identification. However, we note that maxAPEs are over 10%. Again, these maximal errors appear only at the end of the discharge curves.

**Table 5.** Results of the cross-validation of the battery EM parameters on discharge curves performed during Pattern A tests, Pattern B test, and cycle tests #1-3, #2-3, and Append 5 at 0.98 A, and at different levels of battery aging. “Mid” and “Last” indicate the cycle at which the discharge test was performed.

	BoL		Mid		Last	
	MAPE <sub>V</sub> (%)	maxAPE <sub>V</sub> (%)	MAPE <sub>V</sub> (%)	maxAPE <sub>V</sub> (%)	MAPE <sub>V</sub> (%)	maxAPE <sub>V</sub> (%)
<b>Case 1, <math>\delta = 1</math> s</b>						
Pattern A, 25 °C	0.869	13.206	0.917	13.184	0.899	12.520
Pattern A, 0 °C	0.870	13.206	0.946	12.378	0.922	11.154
Pattern B	0.884	13.205	0.857	12.668	0.950	13.537
#1-3	0.978	13.205	1.013	15.288	0.990	14.391
#2-3	0.887	13.205	0.928	13.097	1.280	15.440
Append 5	0.893	13.206	1.051	13.362	1.117	12.501
<b>Case 1, <math>\delta = 5</math> s</b>						
Pattern A, 25 °C	0.870	13.205	0.917	13.184	0.898	12.519
Pattern A, 0 °C	0.870	13.206	0.945	12.376	0.919	11.150
Pattern B	0.884	13.205	0.856	12.667	0.950	13.538
#1-3	0.974	13.205	1.012	15.291	0.990	14.394
#2-3	0.884	13.205	0.928	13.097	1.289	15.445
Append 5	0.891	13.206	1.050	13.362	1.117	12.450
<b>Case 1, <math>\delta = 10</math> s</b>						
Pattern A, 25 °C	0.871	13.206	0.917	13.184	0.895	12.519
Pattern A, 0 °C	0.870	13.206	0.943	12.376	0.916	11.149
Pattern B	0.884	13.205	0.853	12.667	0.948	13.538
#1-3	0.971	13.205	1.010	15.292	0.989	14.395
#2-3	0.882	13.205	0.926	13.097	1.295	15.446
Append 5	0.888	13.206	1.048	13.362	1.116	12.499
<b>Case 2, <math>\delta = 1</math> s</b>						
Pattern A, 25 °C	0.869	13.206	0.916	13.170	0.898	12.502
Pattern A, 0 °C	0.870	13.206	0.944	12.331	0.920	11.114
Pattern B	0.884	13.205	0.855	12.602	0.949	13.495
#1-3	0.978	13.205	1.0113	15.257	0.994	14.511
#2-3	0.887	13.205	0.931	13.152	1.269	15.697
Append 5	0.893	13.206	1.050	13.358	1.121	12.601
<b>Case 2, <math>\delta = 5</math> s</b>						
Pattern A, 25 °C	0.870	13.206	0.917	13.170	0.897	12.500
Pattern A, 0 °C	0.870	13.206	0.943	12.330	0.917	11.109
Pattern B	0.884	13.205	0.853	12.601	0.948	13.496
#1-3	0.974	13.205	1.010	15.260	0.994	14.514
#2-3	0.884	13.205	0.930	13.151	1.277	15.702
Append 5	0.891	13.206	1.049	13.358	1.121	12.600
<b>Case 2, <math>\delta = 10</math> s</b>						
Pattern A, 25 °C	0.871	13.206	0.916	13.170	0.895	12.500
Pattern A, 0 °C	0.870	13.206	0.941	12.329	0.914	11.109
Pattern B	0.884	13.205	0.850	12.600	0.940	13.496
#1-3	0.971	13.205	1.008	15.261	0.992	14.515
#2-3	0.882	13.205	0.929	13.151	1.283	15.704
Append 5	0.888	13.206	1.048	13.358	1.120	12.599

Overall, it is possible to state that the voltage is very well approximated at different temperatures and at different levels of battery aging. The higher errors only appear when the battery cell is deeply discharged, a condition that should be avoided in all practical uses.

### 5.3. Battery Aging Model Parameters

The parameters of the AM were identified applying the methodology presented in Section 4.2 using the experimental results of Experiment 2. After being identified, the AM was validated on the Pattern A tests, on the Pattern B test, and on one of the cycle tests #1-3, #2-3, and Append 5. Similarly to the identification of the battery EM, a sensitivity analysis was conducted on the number of considered capacity and resistance measurements to identify the model parameters. With Case 1, we refer to the case of AM parameter identification conducted using all the available measurements (indicated by a black dot in Figures 10 and 11) whereas we use Case 2 to indicate the case in which half of the available measurements were used, one out of every two, to identify the AM parameters.

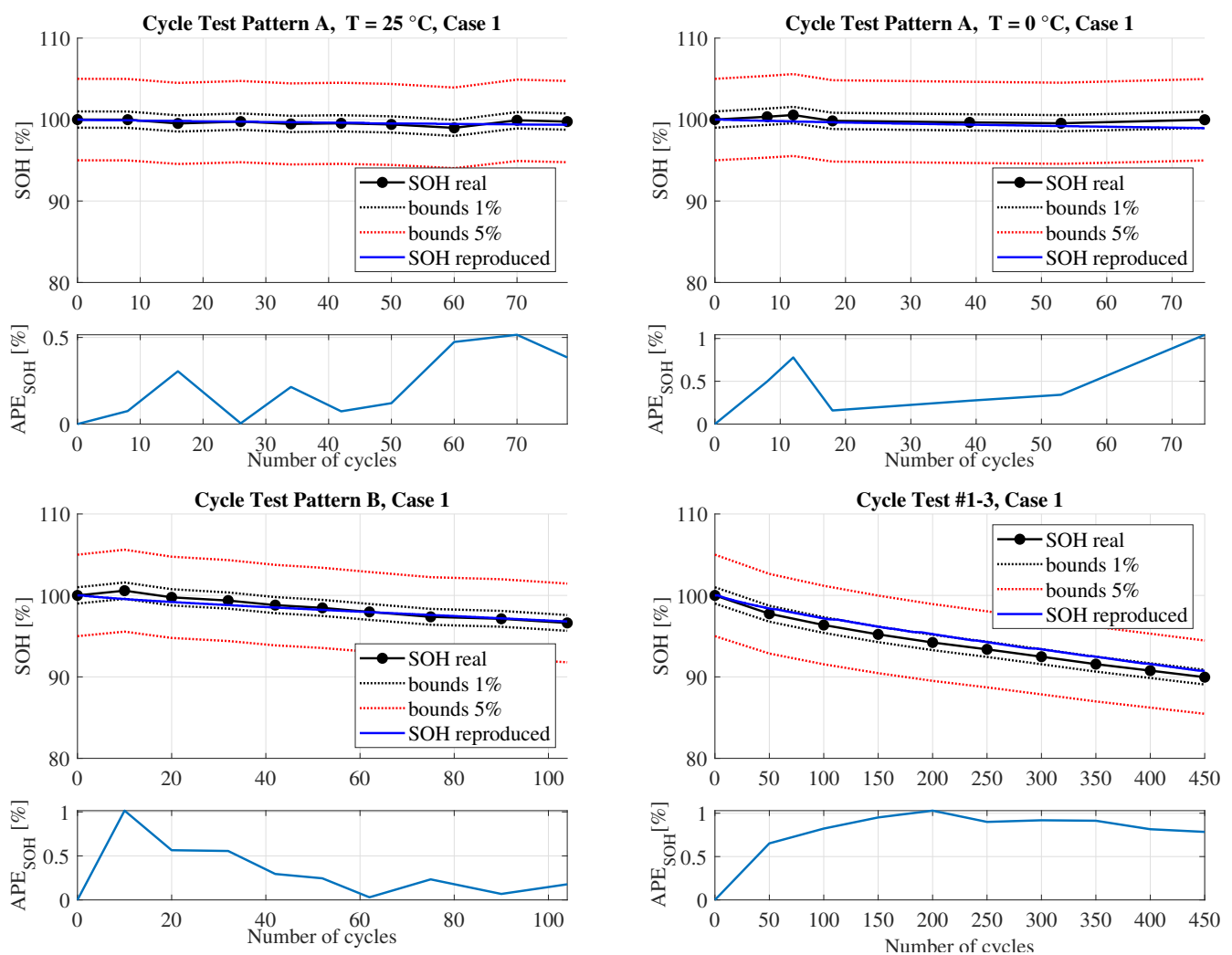
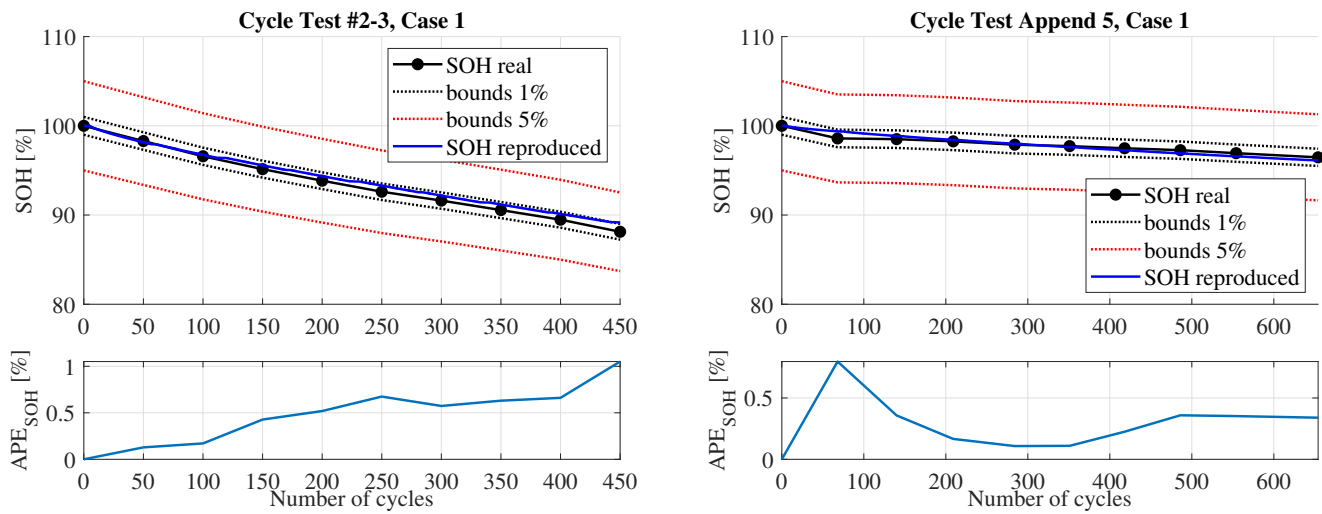
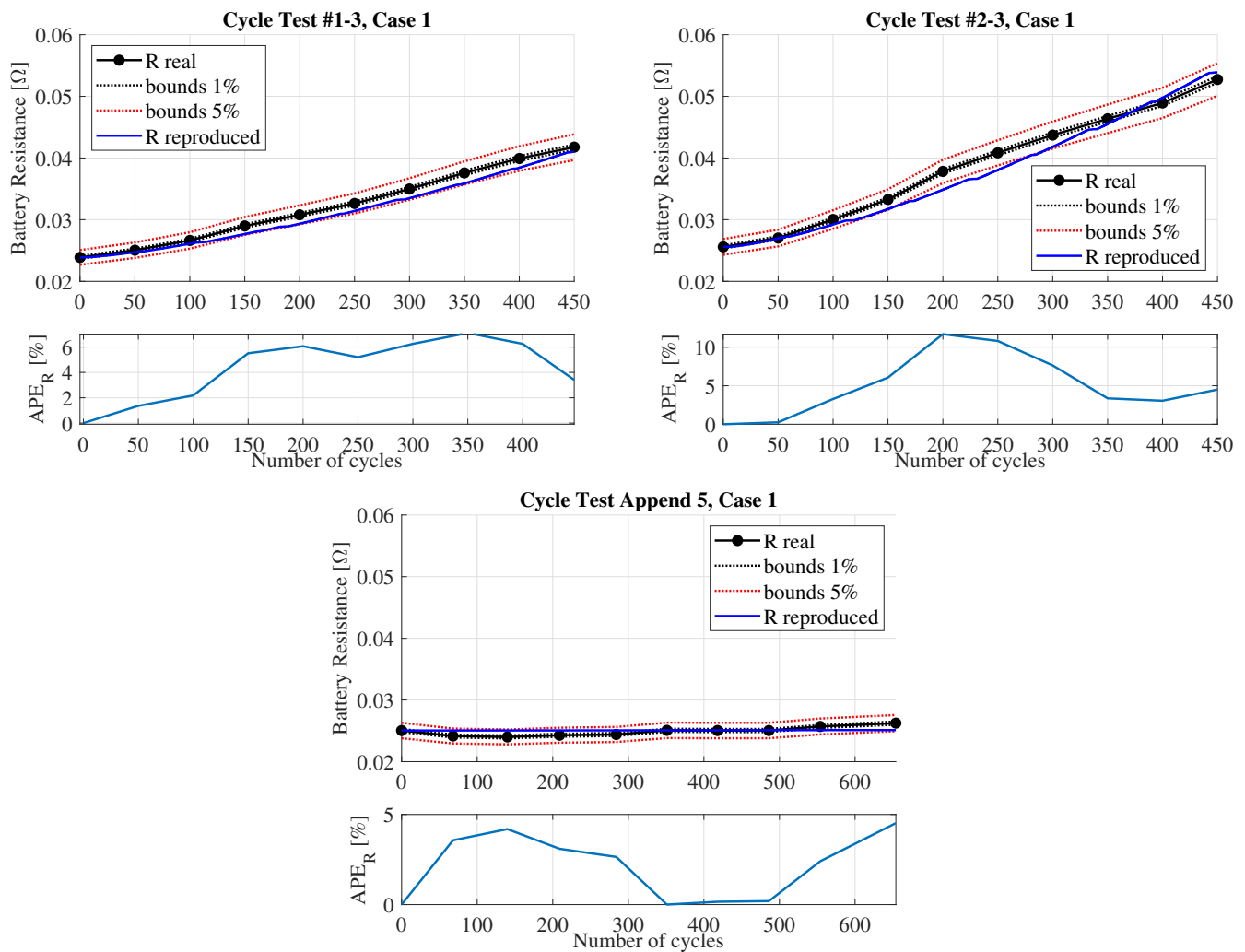


Figure 10. Cont.



**Figure 10.** Results of the battery AM validation for the cell capacity on Pattern A tests, Pattern B test, and cycle tests #1-3, #2-3, and Append 5, for Case 1: SOH percentage levels (top figures) and  $APE_{SOH}$  (bottom figures).



**Figure 11.** Results of the battery AM validation for the cell resistance on cycle tests #1-3, #2-3, and Append 5, for Case 1: battery resistance (top figures) and  $APE_R$  (bottom figures).

Table 6 shows the values of the identified AM parameters for the battery capacity and resistance. The results of the identification of the capacity model parameters are listed in Table 7 in terms of  $MAPE_{SOH}$  and  $maxAPE_{SOH}$ , both for Case 1 and Case 2. Table 7 also shows the performance of the capacity AM obtained in the validation tests. Similarly, Table 8 shows the results of the identification and validation of the resistance parameters in terms of  $MAPE_R$  and  $maxAPE_R$ .

**Table 6.** Estimated values of the battery aging model parameters.

Case	$N_c^{ref}$	$\lambda_Q$	$\lambda_R$	$\psi_Q$	$\gamma_{dQ}$	$\gamma_{cQ}$	$\xi_Q$	$R_{EoL}$	$\psi_R$	$\gamma_{dR}$	$\gamma_{cR}$	$\xi_R$
1	1184	0.7923	1.3507	1685	48.922	48.922	0.1177	0.0830	3055	509,590	127,750	0.0047
2	1213	0.7775	1.4005	1643	38.154	38.154	0.1162	0.0897	2971	345,750	127,750	0.0016

In general, all obtained results prove the effectiveness and the robustness of the proposed approach. Indeed, MAPEs are generally very low and maxAPEs are almost always well below 3%. The validation of the capacity AM shows outstanding results with values of  $MAPE_{SOH}$  significantly lower than 1% and values of  $max(APE_{SOH})$  in the range of 1% or lower. The errors in the validation of the resistance AM are larger. In particular, cycle test #2-3 shows values of  $MAPE_R$  outside the 5% bounds. In the outcome of such results, a big impact comes from the normalization of the error on  $R_{BoL}$  in (59), which is a small value and the minimum in the battery resistance evolution. Such results may be due to some inaccuracy in the resistance measurements tests, which do not consider the battery response dynamics in their computation.

Concerning the difference between Case 1 and Case 2, in Table 6 we can observe that the identification procedure returned different values for the estimated parameters. In any case, the order of magnitude of all parameters is similar and the results in terms of accuracy in Tables 7 and 8 show that the two models have comparable performances.

**Table 7.** Results of the identification and validation of the battery aging model parameters for the battery SOH.

Cycling Condition	Case 1		Case 2	
	$MAPE_{SOH}$ (%)	$maxAPE_{SOH}$ (%)	$MAPE_{SOH}$ (%)	$maxAPE_{SOH}$ (%)
<b>Identification</b>				
#1	0.119	0.614	0.145	0.614
#2	0.129	0.418	0.075	0.218
#3	1.697	3.589	1.721	3.650
#4	0.123	0.370	0.117	0.189
#5	0.236	0.782	0.262	0.782
#6	0.236	0.666	0.196	0.518
<b>Validation</b>				
Pattern A, 25 °C	0.442	1.043	0.215	0.526
Pattern A, 0 °C	0.217	0.515	0.456	1.060
Pattern B	0.318	1.014	0.328	1.034
#1-3	0.779	1.030	0.781	1.009
#2-3	0.484	1.051	0.535	1.215
Append 5	0.281	0.797	0.266	0.782

Figures 10 and 11 graphically show the results of the validation of the battery AM for capacity and resistance, respectively, for Case 1. The same results for Case 2 are not shown, since no significant differences can be appreciated. In Figure 10, we can observe that the SOH evolution of the battery is well represented by the model, since the curves reproduced by the WBM (blue lines) are almost always in the 1% error bounds. In Figure 11, we notice that the reproduction of the battery resistance presents larger percentage errors, as already stated, but in terms of absolute values the largest error is 0.14 mΩ.

**Table 8.** Results of the identification and validation of the battery aging model parameters for the battery resistance.

Cycling Condition	Case 1		Case 2	
	$MAPE_R$ (%)	$\max APE_R$ (%)	$MAPE_R$ (%)	$\max APE_R$ (%)
<b>Identification</b>				
#1	0.062	0.146	0.054	0.146
#2	0.416	0.796	0.469	0.814
#3	0.301	0.606	0.288	0.590
#4	0.604	1.037	0.550	1.053
#5	0.181	0.340	0.180	0.340
#6	0.086	0.215	0.102	0.215
<b>Validation</b>				
#1-3	4.315	7.110	4.093	6.451
#2-3	5.066	11.701	5.629	12.018
Append 5	2.077	4.520	2.077	4.563

## 6. Conclusions

This paper presents a comprehensive Li-ion battery semi-empirical model able to represent the electrothermal dynamics taking into account aging degradation due to operations. Moreover, a suitable procedure to identify both electrothermal and aging parameters is introduced. This method does not require expensive thermal test chambers and calorimeters, since it requires simple cycling and discharge tests. In more detail, the presented model is an integration of two sub-models, the EM, which models the electrical and thermal behavior of the battery, and the AM, which models the aging of the battery through operations. The resulting WBM allows evaluating the battery state of health and resistance temporal evolution as functions of battery temperature, state of charge, and current. Therefore, it can be easily interfaced with a battery management system for the online evaluation of battery conditions.

It is worth remarking that the WBM builds upon existing electrothermal and aging Li-ion cell models. Specifically, the EM is formulated based on the models in [11,24,25], while the AM originates from the framework presented in [20]. However, as already clarified in Sections 3.3 and 4.3, in this paper we introduce two main improvements: the formal inclusion of the relation between the maximum theoretical discharge capacity  $Q_b$ , used in the EM, and the battery nominal capacity  $Q$ , used in the AM; and the generalization of the aging parameter identification procedure to the case of multiple experimental measurements for each aging condition.

The proposed method is validated through experimental tests carried out on real Li-ion battery cells, subject to real load profiles. The identified AM is validated by measuring its capability to estimate the battery state of health in terms of capacity decrease and internal resistance increase. In particular, the results show a MAPE lower than 1% for battery capacity and a maximum absolute error of 0.14 m $\Omega$  for the internal resistance. The identified EM is validated by measuring its capability in reproducing the battery voltage profile both in a fresh battery and at different levels of aging. The results show a MAPE for voltage reproduction lower than 1%.

Notice that the analysis of the performance of the EM at different levels of aging represents a validation of the integration EM-AM in the WBM. This actually addresses a gap in the existing literature, where EM and AM are usually identified and validated separately.

Future works will consider the integration of SOH estimation with a procedure to estimate the battery SOC. Further developments may examine the performance of an adaptive model that updates the parameters during the actual battery operation or consider the design of parameter identification procedures based on a digital-twin approach.



**Author Contributions:** Conceptualization, F.C., M.G. and G.N.; methodology, F.C. and G.N.; software, F.C. and G.N.; validation, F.C. and G.N.; formal analysis, F.C. and G.N.; resources, R.T. and S.T.; data curation, G.N., R.T. and S.T.; writing—original draft preparation, F.C. and G.N.; writing—review and editing, M.G., D.K. and F.S.; supervision, F.C., F.S. and G.V.; project administration, M.G. and G.V. All authors have read and agreed to the published version of the manuscript.

**Funding:** This research received no external funding.

**Data Availability Statement:** The data presented in this study are available on request from the corresponding author. The data are not publicly available due to industrial confidentiality.

**Conflicts of Interest:** M.G. and G.V. were employed by the company Yanmar R&D Europe SRL; R.T. and S.T. were employed by the company Yanmar Holdings Co., Ltd.; the remaining authors declare that the research was conducted in the absence of any commercial or financial relationships that could be construed as a potential conflict of interest.

## List of Symbols

### Variables

$i$	Battery current
$V_b$	Battery voltage
$T$	Battery temperature
$SoC$	Battery state of charge
$i_f$	Filtered battery current

### Varying Parameters

$Q$	Battery capacity
$Q_b$	Battery maximum capacity
$R$	Battery resistance
$E_0$	Battery thermodynamics voltage
$K$	Polarization constant
$A_b$	Battery voltage exponential zone amplitude
$Pol_{res}$	Battery polarization resistance
$\theta$	Stress factor
$\varepsilon$	Aging index
$n$	Number of transitions
$N$	Number of cycles

### Fixed Parameters

$B$	Battery voltage exponential zone time constant
$C$	Battery polarization voltage slope
$V_{full}$	Battery full-capacity voltage
$V_{cut-off}$	Battery cut-off voltage
$T_{ref}$	Battery reference temperature
$N_c^{ref}$	Number of cycles from BoL to EoL at reference cycling conditions
$N_{eq}$	Equivalent number of cycles
EM parameters:	$E_0 _{T_{ref}}, \partial E/\partial T, K _{T_{ref}}, \alpha, R _{T_{ref}}, \beta, Q _{T_{ref}}, \Delta Q/\Delta T, A_b _{T_{ref}}, \partial A_b/\partial T$
AM parameters:	$\lambda_Q, \nu_Q, \psi_Q, \gamma_{dQ}, \gamma_{cQ}, \xi_Q, \lambda_R, \nu_R, \psi_R, \gamma_{dR}, \gamma_{cR}, \xi_R$

## Appendix A

To obtain the relation  $Q(Q_b)$ , we need to solve (5) with respect to  $Q$ . Consider first that the quantity  $A_b \exp(-BQ)$  can be neglected, since usually  $Q > 3/B$  ( $B$  is the inverse of the exponential zone extension). Therefore, from (5), we can obtain the following equation:

$$Q^2 + \frac{V_{cut-off} + Ri_{dis}^{nom} - E_0 - KQ_b - CQ_b}{C}Q - \frac{Ri_{dis}^{nom} + Ki_{dis}^{nom} + V_{cut-off} - E_0}{C}Q_b = 0 \quad (A1)$$

It is easy to demonstrate that, for  $K > 0$  and  $V_{full} > V_{cut-off}$ , (A1) has two real solutions, with at least one solution positive. Indeed, by its own definition, (A1) is satisfied with real solutions if and only if the discharge curve in Figure 6 crosses the cut-off voltage  $V_{cut-off}$ . It is obvious that with  $K > 0$  and  $V_{full} > V_{cut-off}$  this is guaranteed. Nevertheless, to obtain the relation  $Q(Q_b)$ , we need to select the right one among the two real solutions. To this end, the following procedure can be followed:

If both solutions are positive, two scenarios can take place:

1. Both solutions are smaller than  $Q_b$ , i.e., the discharge curve crosses the cut-off voltage  $V_{cut-off}$  twice before the negative asymptote in  $Q_b$ ; that means the right solution to consider is the largest;
2. One solution is larger and one is smaller than  $Q_b$ , i.e., the discharge curve crosses the cut-off voltage one time before the negative asymptote in  $Q_b$  and one after the asymptote; in this case, the right solution to consider is the smallest.

If one solution is positive and one is negative, the right solution to consider is the positive one.

## Appendix B

In this appendix, we provide further details on the function  $g_k^T(\cdot)$  used in (32). This function is used to estimate the subsets of parameters  $\{\varphi_{in}\}_\kappa$ , given the sets  $\{\varphi_{in}^T\}_{T=T_1}^{T_r}$ . The subscript  $\kappa$  refers to a specific subset of parameters in  $\varphi$ :

- $\{\varphi\}_1 = \{E_0|_{T_{ref}}, \partial E/\partial T\}$ ;
- $\{\varphi\}_2 = \{K|_{T_{ref}}, \alpha\}$ ;
- $\{\varphi\}_3 = \{R|_{T_{ref}}, \beta\}$ ;
- $\{\varphi\}_4 = \{A_b|_{T_{ref}}, \partial A_b/\partial T\}$ ;
- $\{\varphi\}_5 = \{Q_b|_{T_{ref}}, \Delta Q/\Delta T\}$ ;
- $\{\varphi\}_6 = \{B\}$ ;
- $\{\varphi\}_7 = \{C\}$ .

For  $\kappa = 1, 4, 5$ ,  $g_k^T(\cdot)$  is defined as follows:

$$g_k^T(x_1, x_2) = x_1 + x_2(T - T_{ref}); \quad (A2)$$

for  $\kappa = 2, 3$ ,  $g_k^T(\cdot)$  is defined as follows:

$$g_k^T(x_1, x_2) = x_1 \exp\left(x_2 \left(\frac{1}{T} - \frac{1}{T_{ref}}\right)\right); \quad (A3)$$

for  $\kappa = 6, 7$ ,  $g_k^T(\cdot)$  is defined as follows:

$$g_k^T(x) = x. \quad (A4)$$

## References

1. Zubi, G.; Dufo-López, R.; Carvalho, M.; Pasaoglu, G. The lithium-ion battery: State of the art and future perspectives. *Renew. Sustain. Energy Rev.* **2018**, *89*, 292–308. [\[CrossRef\]](#)
2. Chen, X.; Shen, W.; Vo, T.T.; Cao, Z.; Kapoor, A. An overview of lithium-ion batteries for electric vehicles. In Proceedings of the 10th International Power and Energy Conference (IPEC 2012), Ho Chi Minh City, Vietnam, 12–14 December 2012; pp. 230–235.
3. Liang, Y.; Zhao, C.Z.; Yuan, H.; Chen, Y.; Zhang, W.; Huang, J.Q.; Yu, D.; Liu, Y.; Titirici, M.M.; Chueh, Y.L.; et al. A review of rechargeable batteries for portable electronic devices. *InfoMat* **2019**, *1*, 6–32. [\[CrossRef\]](#)
4. Chen, T.; Jin, Y.; Lv, H.; Yang, A.; Liu, M.; Chen, B.; Xie, Y.; Chen, Q. Applications of Lithium-Ion Batteries in Grid-Scale Energy Storage Systems. *Trans. Tianjin Univ.* **2020**, *26*, 208–217. [\[CrossRef\]](#)
5. Gielen, D.; Boshell, F.; Saygin, D.; Bazilian, M.D.; Wagner, N.; Gorini, R. The role of renewable energy in the global energy transformation. *Energy Strategy Rev.* **2019**, *24*, 38–50. [\[CrossRef\]](#)

6. Battery University. Comparison of Secondary Batteries. Available online: <https://batteryuniversity.com/article/bu-107-comparison-table-of-secondary-batteries> (accessed on 24 April 2024).
7. Uno, M.; Kukita, A. Cycle Life Evaluation Based on Accelerated Aging Testing for Lithium-Ion Capacitors as Alternative to Rechargeable Batteries. *IEEE Trans. Ind. Electron.* **2016**, *63*, 1607–1617. [\[CrossRef\]](#)
8. McCurlie, L.; Preindl, M.; Emadi, A. Fast Model Predictive Control for Redistributive Lithium-Ion Battery Balancing. *IEEE Trans. Ind. Electron.* **2017**, *64*, 1350–1357. [\[CrossRef\]](#)
9. Liu, L.; Park, J.; Lin, X.; Sastry, A.M.; Lu, W. A thermal-electrochemical model that gives spatial-dependent growth of solid electrolyte interphase in a Li-ion battery. *J. Power Sources* **2014**, *268*, 482–490. [\[CrossRef\]](#)
10. Li, J.; Wang, L.; Lyu, C.; Liu, E.; Xing, Y.; Pecht, M. A parameter estimation method for a simplified electrochemical model for Li-ion batteries. *Electrochim. Acta* **2018**, *275*, 50–58. [\[CrossRef\]](#)
11. Motapon, S.N.; Lupien-Bedard, A.; Dessaint, L.A.; Fortin-Blanchette, H.; Al-Haddad, K. A Generic Electrothermal Li-ion Battery Model for Rapid Evaluation of Cell Temperature Temporal Evolution. *IEEE Trans. Ind. Electron.* **2017**, *64*, 998–1008. [\[CrossRef\]](#)
12. Atalay, S.; Sheikh, M.; Mariani, A.; Merla, Y.; Bower, E.; Widanage, W.D. Theory of battery ageing in a lithium-ion battery: Capacity fade, nonlinear ageing and lifetime prediction. *J. Power Sources* **2020**, *478*, 229026. [\[CrossRef\]](#)
13. Li, J.; Adewuyi, K.; Lotfi, N.; Landers, R.G.; Park, J. A single particle model with chemical/mechanical degradation physics for lithium ion battery State of Health (SOH) estimation. *Appl. Energy* **2018**, *212*, 1178–1190. [\[CrossRef\]](#)
14. Li, J.; Lotfi, N.; Landers, R.G.; Park, J. A Single Particle Model for Lithium-Ion Batteries with Electrolyte and Stress-Enhanced Diffusion Physics. *J. Electrochem. Soc.* **2017**, *164*, A874. [\[CrossRef\]](#)
15. Lucu, M.; Martinez-Laserna, E.; Gandiaga, I.; Liu, K.; Camblong, H.; Widanage, W.; Marco, J. Data-driven nonparametric Li-ion battery ageing model aiming at learning from real operation data—Part A: Storage operation. *J. Energy Storage* **2020**, *30*, 101409. [\[CrossRef\]](#)
16. Lucu, M.; Martinez-Laserna, E.; Gandiaga, I.; Liu, K.; Camblong, H.; Widanage, W.; Marco, J. Data-driven nonparametric Li-ion battery ageing model aiming at learning from real operation data—Part B: Cycling operation. *J. Energy Storage* **2020**, *30*, 101410. [\[CrossRef\]](#)
17. Tang, X.; Liu, K.; Wang, X.; Gao, F.; MacRo, J.; Widanage, W.D. Model Migration Neural Network for Predicting Battery Aging Trajectories. *IEEE Trans. Transp. Electr.* **2020**, *6*, 363–374. [\[CrossRef\]](#)
18. Bertinelli Salucci, C.; Bakdi, A.; Glad, I.K.; Vanem, E.; De Bin, R. Multivariable Fractional Polynomials for lithium-ion batteries degradation models under dynamic conditions. *J. Energy Storage* **2022**, *52*, 104903. [\[CrossRef\]](#)
19. Park, S.W.; Lee, H.; Won, Y.S. A novel aging parameter method for online estimation of Lithium-ion battery states of charge and health. *J. Energy Storage* **2022**, *48*, 103987. [\[CrossRef\]](#)
20. Motapon, S.N.; Lachance, E.; Dessaint, L.A.; Al-Haddad, K. A Generic Cycle Life Model for Lithium-Ion Batteries Based on Fatigue Theory and Equivalent Cycle Counting. *IEEE Open J. Ind. Electron. Soc.* **2020**, *1*, 207–217. [\[CrossRef\]](#)
21. Varini, M.; Campana, P.E.; Lindbergh, G. A semi-empirical, electrochemistry-based model for Li-ion battery performance prediction over lifetime. *J. Energy Storage* **2019**, *25*, 100819. [\[CrossRef\]](#)
22. Xu, B.; Oudalov, A.; Ulbig, A.; Andersson, G.; Kirschen, D.S. Modeling of Lithium-Ion Battery Degradation for Cell Life Assessment. *IEEE Trans. Smart Grid* **2018**, *9*, 1131–1140. [\[CrossRef\]](#)
23. Xue, Y.; Zhou, H.; Luo, Y.; Lam, J. Battery Degradation Modelling and Prediction with Combination of Machine Learning and Semi-empirical Methods. In Proceedings of the 2022 12th International Conference on Power, Energy and Electrical Engineering (CPEEE 2022), Shiga, Japan, 25–27 February 2022.
24. Tremblay, O.; Dessaint, L.A.; Dekkiche, A.I. A generic battery model for the dynamic simulation of hybrid electric vehicles. In Proceedings of the VPPC 2007—Proceedings of the 2007 IEEE Vehicle Power and Propulsion Conference, Arlington, TX, USA, 9–12 September 2007.
25. Tremblay, O.; Dessaint, L.A. Experimental Validation of a Battery Dynamic Model for EV Applications. *World Electr. Veh. J.* **2009**, *3*, 289–298. [\[CrossRef\]](#)
26. Zhang, F.; Xiao, L.; Coskun, S.; Pang, H.; Xie, S.; Liu, K.; Cui, Y. Comparative study of energy management in parallel hybrid electric vehicles considering battery ageing. *Energy* **2023**, *264*, 123219. [\[CrossRef\]](#)
27. Ma, Z.; Luan, Y.; Zhang, F.; Xie, S.; Coskun, S. A data-driven energy management strategy for plug-in hybrid electric buses considering vehicle mass uncertainty. *J. Energy Storage* **2024**, *77*, 109963. [\[CrossRef\]](#)
28. Amini, M.; Khorsandi, A.; Vahidi, B.; Hosseinian, S.H.; Malakmahmoudi, A. Optimal sizing of battery energy storage in a microgrid considering capacity degradation and replacement year. *Electr. Power Syst. Res.* **2021**, *195*, 107170. [\[CrossRef\]](#)
29. Alsaidan, I.; Khodaei, A.; Gao, W. A comprehensive battery energy storage optimal sizing model for microgrid applications. *IEEE Trans. Power Syst.* **2017**, *33*, 3968–3980. [\[CrossRef\]](#)
30. Wankmüller, F.; Thimmapuram, P.R.; Gallagher, K.G.; Botterud, A. Impact of battery degradation on energy arbitrage revenue of grid-level energy storage. *J. Energy Storage* **2017**, *10*, 56–66. [\[CrossRef\]](#)
31. Han, X.; Lu, L.; Zheng, Y.; Feng, X.; Li, Z.; Li, J.; Ouyang, M. A review on the key issues of the lithium ion battery degradation among the whole life cycle. *eTransportation* **2019**, *1*, 100005. [\[CrossRef\]](#)
32. Samsung. Samsung INR21700-50E 5000mAh (Cyan). Available online: [https://lygte-info.dk/review/batteries2012/SamsungINR21700-50E5000mAh\(Cyan\)UK.html](https://lygte-info.dk/review/batteries2012/SamsungINR21700-50E5000mAh(Cyan)UK.html) (accessed on 24 April 2024).
33. Yanmar Holdings Co., Ltd. Available online: <https://www.yanmar.com/global/> (accessed on 24 April 2024).

34. Shepherd, C.M. Design of Primary and Secondary Cells: II. An Equation Describing Battery Discharge. *J. Electrochem. Soc.* **1965**, *112*, 657. [[CrossRef](#)]
35. Rasmann, E.; Baker, K.; Shi, Y.; Christensen, D. Modeling stationary lithium-ion batteries for optimization and predictive control. In Proceedings of the 2017 IEEE Power and Energy Conference at Illinois (PECI 2017), Champaign, IL, USA, 23–24 February 2017.
36. Troxler, Y.; Wu, B.; Marinescu, M.; Yufit, V.; Patel, Y.; Marquis, A.J.; Brandon, N.P.; Offer, G.J. The effect of thermal gradients on the performance of lithium-ion batteries. *J. Power Sources* **2014**, *247*, 1018–1025. [[CrossRef](#)]

**Disclaimer/Publisher’s Note:** The statements, opinions and data contained in all publications are solely those of the individual author(s) and contributor(s) and not of MDPI and/or the editor(s). MDPI and/or the editor(s) disclaim responsibility for any injury to people or property resulting from any ideas, methods, instructions or products referred to in the content.